 Open access • Posted Content • DOI:10.1101/824995

## Innate Antifungal Immune Receptor, Dectin-1, Undergoes Ligand-Induced Oligomerization with Highly Structured $\beta$ -Glucans and at Fungal Cell Contact Sites

— [Source link](#) 

Eduardo U. Anaya, Akram Etemadi Amin, Mike Danielson, Kyle S. Michel ...+1 more authors





**Institutions:** University of New Mexico

**Published on:** 30 Oct 2019 - bioRxiv (Cold Spring Harbor Laboratory)

**Topics:** Glucan, Receptor Aggregation, Immune receptor, Ligand (biochemistry) and Receptor

Related papers:

- [Structure of the Fungal Beta-Glucan-Binding Immune Receptor Dectin-1: Implications for Function.](#)
- [Innate Antifungal Immune Receptor, Dectin-1, Undergoes Ligand-Induced Oligomerization with Highly Structured  \$\beta\$ -glucans and at Fungal Cell Contact Sites](#)
- [C-type lectin receptors Dectin-3 and Dectin-2 form a heterodimeric pattern-recognition receptor for host defense against fungal infection.](#)
- [Cellular and molecular mechanisms of fungal  \$\beta\$ -\(1 \$\rightarrow\$ 6\)-glucan in macrophages.](#)
- [A computational model for regulation of nanoscale glucan exposure in \*Candida albicans\*.](#)

Share this paper:    

View more about this paper here: <https://typeset.io/papers/innate-antifungal-immune-receptor-dectin-1-undergoes-ligand-1y3zheql3>

1 **Dectin-1 Molecular Aggregation and Signaling is Sensitive to  $\beta$ -Glucan Structure**  
2 **and Glucan Exposure on *Candida albicans* Cell Walls**

3

4 Authors:

5 **Eduardo U. Anaya<sup>1</sup>, Akram Etemadi Amin<sup>1,2</sup>, Michael J. Wester<sup>3</sup>, Michael E.**  
6 **Danielson<sup>4</sup>, Kyle S. Michel<sup>4</sup>, Aaron K. Neumann<sup>1,5</sup>**

7 Affiliations:

8 1. Department of Pathology, University of New Mexico, School of Medicine,

9 Albuquerque, NM, USA, 87131

10 2. Department of Physics and Astronomy, University of New Mexico, Albuquerque, NM,

11 USA 87131

12 3. Department of Mathematics and Statistics, University of New Mexico, Albuquerque,

13 NM, USA, 87131

14 4. ImmunoResearch Inc., Eagan, MN, USA, 55121

15 5. Corresponding author: [akneumann@salud.unm.edu](mailto:akneumann@salud.unm.edu)

16

17 **Keywords:**

18 Dectin-1, dimer,  $\beta$ -Glucan, *Candida albicans*, hemITAM, Syk, Calcium signaling,

19 (Förster Resonance Energy Transfer) FRET, Raster Image Correlation Spectroscopy

20 (RICS), Numbers & Brightness analysis (N&B)

21

## 22 **Abstract**

23 Dectin-1A is a C-type Lectin innate immunoreceptor that recognizes  $\beta$ -(1,3;1,6)-glucan,  
24 a structural component of *Candida* species cell walls. The higher order structure of  $\beta$ -  
25 glucans ranges from random coil to insoluble fiber due to varying degrees of tertiary  
26 (helical) and quaternary structure. Model *Saccharomyces cerevisiae*  $\beta$ -glucans of  
27 medium and high molecular weight (MMW and HMW, respectively) are highly  
28 structured. In contrast, low MW glucan (LMW) is much less structured. Despite similar  
29 affinity for Dectin-1A, the ability of glucans to induce Dectin-1A mediated calcium influx  
30 and Syk phosphorylation positively correlates with their degree of higher order structure.  
31 Chemical denaturation and renaturation of MMW glucan showed that glucan structure  
32 determines agonistic potential, but not binding affinity, for Dectin-1A. We explored the  
33 role of glucan structure on Dectin-1A oligomerization, which is thought to be required for  
34 Dectin-1 signaling. Glucan signaling decreased Dectin-1A diffusion coefficient in inverse  
35 proportion to glucan structural content, which was consistent with Dectin-1A  
36 aggregation. Förster Resonance Energy Transfer (FRET) measurements revealed that  
37 molecular aggregation of Dectin-1 occurs in a manner dependent upon glucan higher  
38 order structure. Number and Brightness analysis specifically confirmed an increase in  
39 the Dectin-1A dimer and oligomer populations that is correlated with glucan structure  
40 content. Comparison of receptor modeling data with FRET measurements confirms that  
41 in resting cells, Dectin-1A is predominantly in a monomeric state. Super Resolution  
42 Microscopy revealed that glucan-stimulated Dectin-1 aggregates are very small (<15  
43 nm) collections of a few engaged receptors. Finally, FRET measurements confirmed  
44 increased molecular aggregation of Dectin-1A at fungal particle contact sites in a

45 manner that positively correlated with the degree of exposed glucan on the particle  
46 surface. These results indicate that Dectin-1A senses the solution conformation of  $\beta$ -  
47 glucans through their varying ability to drive receptor dimer/oligomer formation and  
48 activation of membrane proximal signaling events.

49

## 50 **Introduction**

51 Overall, *Candida* infections have increased over the past 20 years in the United States  
52 [1–5]. It is estimated that 46,000 cases of healthcare-associated invasive candidiasis  
53 occur in the United States annually [6]. The fungal cell wall is composed of an inner  
54 layer of chitin, a middle layer of  $\beta(1,3;1,6)$ -D-glucan and an outer layer of N- and O-  
55 linked mannans [7]. During infection, the cell wall of *Candida* is an important and  
56 relevant virulence factor, playing roles in adhesion, colonization and immune recognition  
57 [8,9].

58 Due to the abundant amount of mannan in the outer cell wall,  $\beta$ -glucan exhibits a very  
59 limited, punctate pattern of nanoscale surface exposure. The extent of this glucan  
60 masking is influenced by environmental conditions such as intestinal pH or lactate levels  
61 [10,11]. In addition, interactions with neutrophils have been shown to “unmask” the  
62 mannose layer through a neutrophil extracellular trap-mediated mechanism [12].  
63 Furthermore, our lab and others have determined that anti-fungal drugs “unmask” the  
64 fungal cell wall, which leads to increases in nanoscale regions of glucan exposure and  
65 correlates with enhanced host defense [13–15]. Therefore, fungal species use masking  
66 as a way to evade immune recognition of  $\beta$ -glucan by the host’s immune system [16].

67  $\beta$ -glucans consist of a  $\beta$ -1,3-linked backbone with side chains of  $\beta$ -1,6-linked units that  
68 vary in length and degree of branching [17].  $\beta$ -glucan forms triple-helical structures  
69 through intermolecular hydrogen bonds with two other strands [17–21]. This triple helix  
70 conformation is shown to form with just the  $\beta$ -1,3-linked backbone, however  $\beta$ -1,6-linked  
71 side chains play an important role in determination of the triple helix cavity formation  
72 through side chain/side chain interactions [21].

73  $\beta$ -glucans are known for their biological activities such as enhancing anti-tumor, anti-  
74 bacterial, and anti-viral immunity as well as wound healing [22–25]. The biological  
75 activity of glucan is affected by its structure, size, structural modification, conformation  
76 and solubility [26]. Research has found that branching is not required to observe  
77 biological activity, but branching has been shown to enhance binding to the Dectin-1  
78 receptor [27]. In contrast,  $\beta$ -glucan size is thought to play a major role in biological  
79 activity with glucans that are shorter than 10,000 Da being generally inactive *in vivo*  
80 [28,29]. However, despite having similar sizes, glucans can display differences in their  
81 biological activities [30–32]. For example, studies have demonstrated that the  
82 immunoregulatory activity of variously sourced laminarin ranges from agonistic to  
83 antagonistic depending on its physicochemical properties, purity and structure [33].

84 Furthermore,  $\beta$ -glucans that have a triple helical conformation are more potent agonists  
85 of host immune response than single helical glucan [27,34–36]. We propose that the  $\beta$ -  
86 glucan triple-helix conformation plays an important role in determining the biological  
87 activity of the  $\beta$ -glucan through modulating the degree of receptor oligomerization upon  
88 ligation.

89 During innate immune recognition of *Candida*, the organization of cell wall ligands and  
90 pattern recognition receptors is an important determinant of successful immune  
91 activation [8]. The fungi-responsive C-type lectin (CTL) anti-fungal immunoreceptors  
92 play a central role in the detection of *Candida* [37]. Human Dectin-1A is the main CTL  
93 that recognizes the  $\beta$ -glucan found in the fungal cell wall [38–40]. Dectin-1A is found in  
94 myeloid lineage cells, and once activated, it stimulates phagocytic activity, the  
95 production of reactive oxygen intermediates and inflammatory mediators. Dectin-1A  
96 contains a CTL-like domain, separated from the cell membrane by a glycosylated stalk  
97 region, a transmembrane domain and an intracellular cytosolic domain. Dectin-1  
98 contains half an Immunoreceptor Tyrosine-based Activation Motif (a YXXL sequence  
99 with an upstream stretch of acidic amino acids) in its cytoplasmic tail, which is termed a  
100 (hem)ITAM domain [41,42]. Monophosphorylated ITAM domains, which are anticipated  
101 to approximate the structure of phosphorylated (hem)ITAM domains, poorly recruit and  
102 activate Syk for downstream signaling because they cannot support bivalent  
103 engagement of both of Syk's SH2 domains [43]. Another (hem)ITAM bearing receptor,  
104 CLEC-2, is reported to require dimerization for its signaling [44]. By analogy to this and  
105 other (hem)ITAM receptors, it is speculated that Dectin-1A must oligomerize to  
106 recapitulate a multivalent binding site for Syk to facilitate signal transduction [8,44,45].  
107 However, this prediction has not been directly explored for Dectin-1A in live cells at the  
108 molecular level with relation to signaling outcomes.

109 In this study, we propose that factors that induce an aggregated membrane organization  
110 of Dectin-1A during activation are very important for determining signaling outcomes of  
111 Dectin-1A engagement by  $\beta$ -glucan [44,45]. We hypothesize that ligand structure, at the

112 levels of glucan tertiary and quaternary structure as well as nanoscale glucan  
113 exposures on the pathogen surface, impacts signaling by determining the membrane  
114 organization and spatiotemporal clustering dynamics of Dectin-1A. To test this  
115 hypothesis, we stimulated HEK-293 cells transfected with Dectin-1A with a variety of  
116 soluble  $\beta$ -glucans that have different structures and sizes. We chose to work in this  
117 model system because it provides a simplified platform necessary to investigate the  
118 physical biology of Dectin-1A activation by isolating Dectin-1A signaling from the  
119 complex milieu of other receptors and other Dectin-1 isoforms expressed in innate  
120 immunocytes. Also, this model facilitates the expression of multiple fluorescent protein-  
121 tagged Dectin-1A constructs necessary to the work. Using calcium imaging and western  
122 blotting assays, our results revealed that Dectin-1A activation is influenced by the  $\beta$ -  
123 glucan triple helical structure. Furthermore, our subcellular FRET measurements by  
124 Fluorescence Lifetime Imaging Microscopy (FLIM-FRET), as well as application of  
125 fluorescence correlation spectroscopy approaches, revealed dimerization and  
126 oligomerization of Dectin-1A when stimulated with highly structured  $\beta$ -glucans. In  
127 addition, these dimerization events occurred in fungal contact sites of fungal cells with  
128 high glucan exposure. Together, our findings indicate  $\beta$ -glucan structure is required for  
129 Dectin-1A to form dimeric and oligomeric membrane aggregates.

130

## 131 **Results**

132 **Dectin-1A activation is dependent on the molecular weight of the soluble  $\beta$ -**  
133 **glucan.**

134  $\beta$ -glucans, existing as insoluble fibers in the cell wall, are likely to have a high degree of  
135 tertiary and quaternary structure. So, an encounter with highly structured glucan might  
136 be indicative of a pathogen cell wall structure. Furthermore, less structured glucans are  
137 encountered by Dectin-1A physiologically [41]. Small soluble circulating glucan can  
138 derive from sloughed cell wall material or from dietary absorption [46–49]. However,  
139 there is not much known about Dectin-1A’s ability to distinguish between highly  
140 structured  $\beta$ -glucan found on cell walls of fungal pathogens and less structured glucans  
141 found in circulation. Therefore, we examined how Dectin-1A activation is affected by  
142 glucans with different quaternary and tertiary structures. To accomplish this, we used  
143 high molecular weight (HMW 450 kDa), medium molecular weight (MMW 145 kDa), and  
144 low molecular weight (LMW 11 kDa) soluble glucans, in decreasing order of tertiary and  
145 quaternary structures, derived from *S. cerevisiae* cell walls. These *S. cerevisiae* glucans  
146 in soluble form or as particulate “zymosan” are common models for stimulation of innate  
147 immunocytes by fungal pathogen cell wall glucan. The above glucans have overall very  
148 similar composition and structures to *C. albicans* yeast glucan, though relatively minor  
149 differences in  $\beta$ -(1,6)-glucan side chain length and branching frequency have been  
150 reported between these species [50,51].

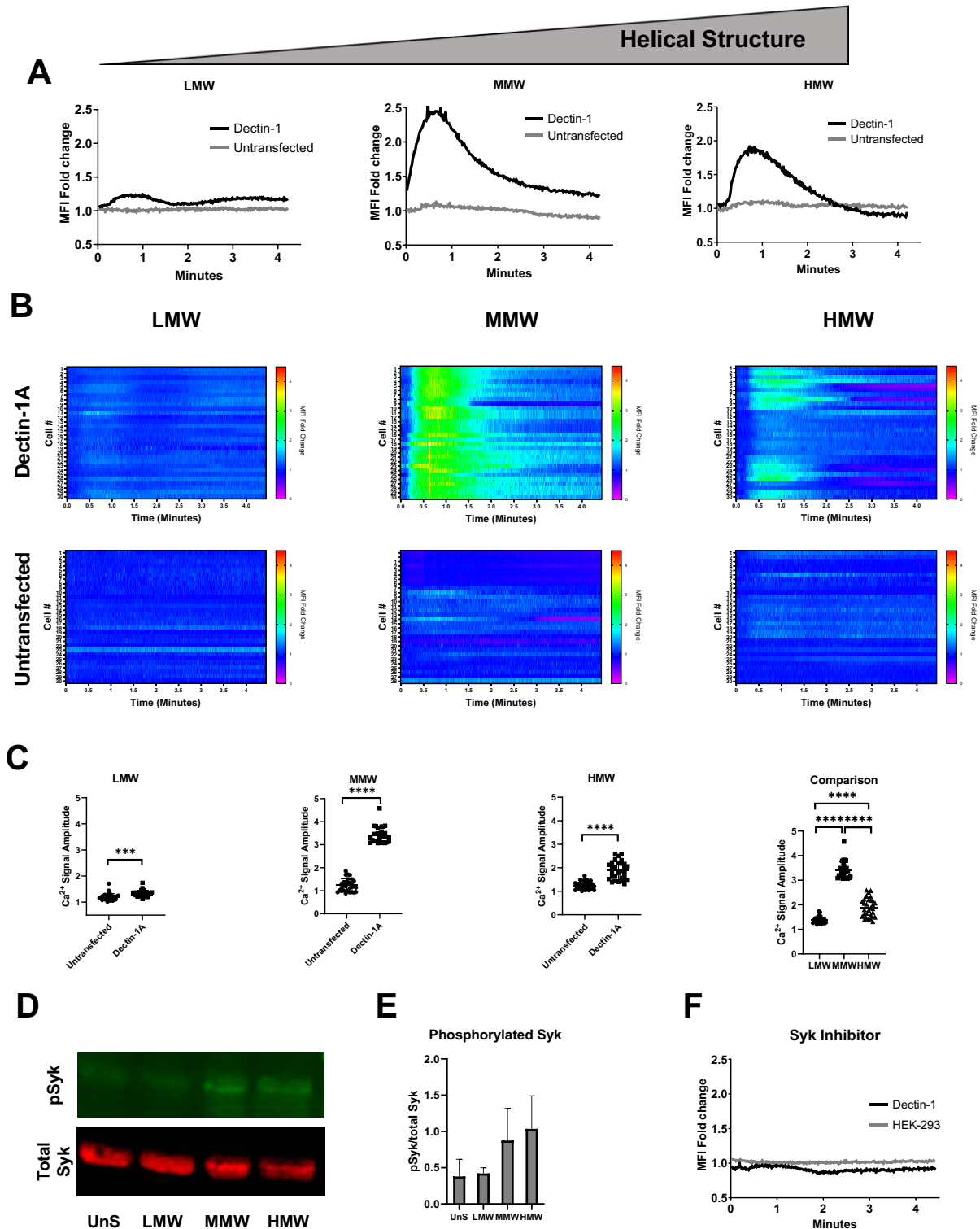
151 Using these glucans, we performed intracellular calcium ( $[Ca^{2+}]_i$ ) measurement  
152 experiments on HEK-293 cells (lacking endogenous Dectin-1 expression) transfected  
153 with Dectin-1A. We stimulated the cells using either LMW, MMW, or HMW glucan. All  
154 the glucans induced a significant increase in peak amplitude  $[Ca^{2+}]_i$  compared to  
155 unstimulated cells (Fig.1 A,B). We found that large, highly ordered glucans (HMW and  
156 MMW) induced a significant, Dectin-1 dependent increase in peak amplitude of  $[Ca^{2+}]_i$



157 compared to LMW, with MMW having the highest peak amplitude (Fig. 1C).  
158 Interestingly, the response to MMW glucan was uniform at the single cell level.  
159 However, cells stimulated with HMW glucan exhibited a more heterogeneous response,  
160 with some cells achieving comparable maximum amplitudes as with MMW and others  
161 exhibiting little change from basal calcium levels (Fig. 1A, B). We expect that HMW  
162 glucan is present as larger particles than MMW, so at equal mass/volume  
163 concentrations, the HMW solution will have a lower concentration of particles. Non-  
164 responder cells in HMW experiments may have stochastically encountered too few  
165 glucan particles to achieve a detectable signaling response. When we stimulated cells  
166 with MMW or HMW at equimolar concentrations, which should have similar glucan  
167 particulate concentrations, we observed a minor difference in peak amplitude, but we  
168 saw that the integrated  $\text{Ca}^{2+}$  flux over time was the same for MMW and HMW glucans  
169 (Supplemental Fig. 1). Furthermore, single cell data demonstrated a similarly uniform  
170 response of Dectin-1 to MMW and HMW glucans under these conditions. These results  
171 indicate that Dectin-1A drives differential  $\text{Ca}^{2+}$  flux to glucan ligands that vary in size  
172 and structure.

173 To determine how these differently-structured, soluble glucans impacted cellular  
174 patterns of Syk phosphorylation, we stimulated HEK-293 cells expressing Dectin1A-  
175 mEmerald with  $\text{H}_2\text{O}$  (vehicle), LMW, MMW, or HMW. Whole cell lysate was collected  
176 and Syk phosphorylation was determined by western blot analysis. Likewise, our results  
177 show an increase in Syk phosphorylation in the larger, highly structured glucan MMW  
178 and HMW compared to unstimulated and LMW stimulated cells (Fig. 1 D,E).  
179 Additionally, Syk inhibitors abrogated calcium signaling of Dectin-1A when stimulated

180 with MMW glucan (Fig. 1F). These results indicate that glucans with higher order  
181 structure are better able to activate Dectin-1A-mediated  $\text{Ca}^{2+}$  signaling and that this is a  
182 Syk dependent process.



183

184 **Figure 1. Differential signaling response of Dectin-1A to soluble  $\beta$ -glucan.**

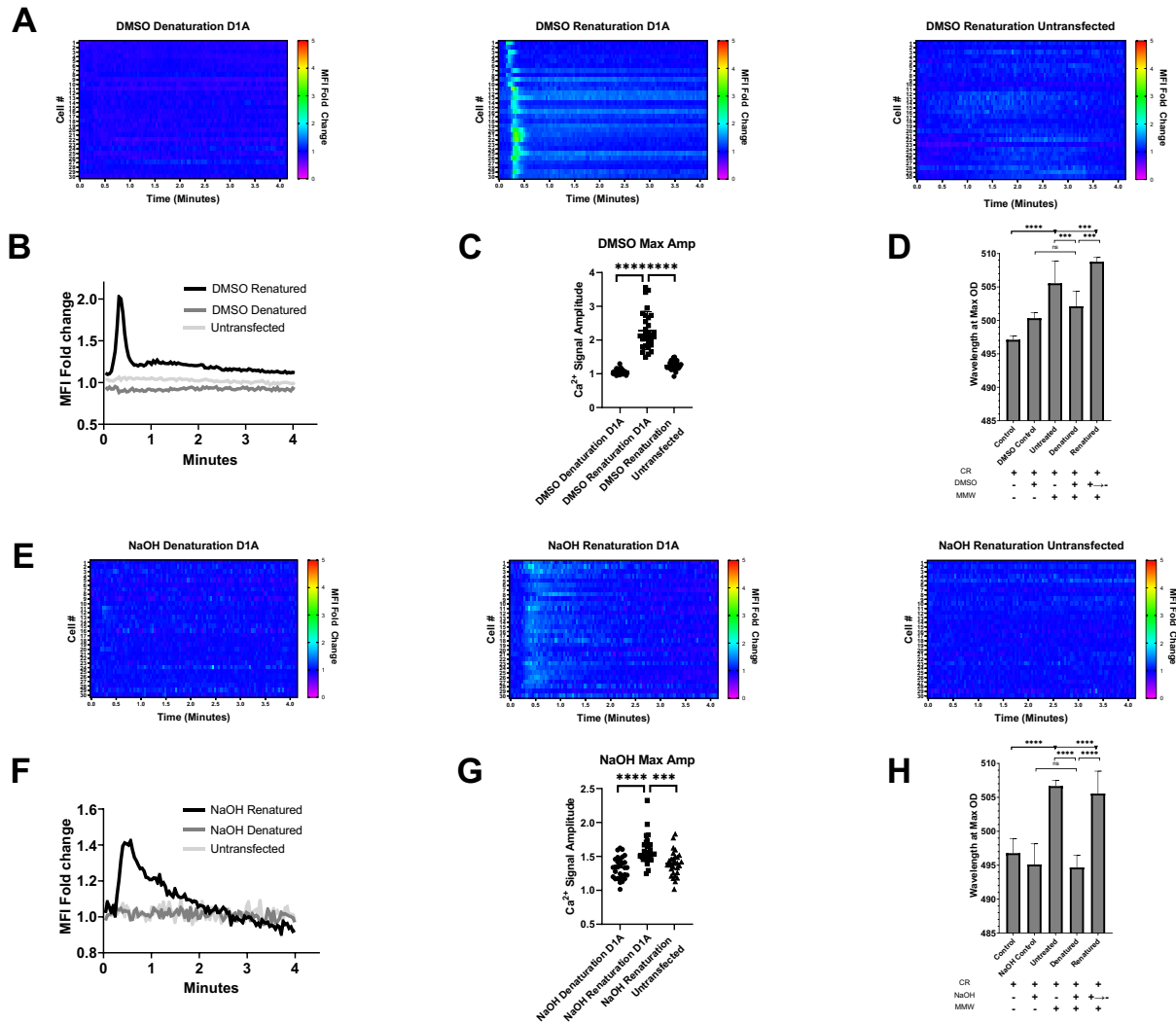
185 (A) HEK-293 cells stably transfected with Dectin-1A were loaded with Fluo-4 and Cell Tracker Deep Red  
186 at equimolar concentrations. Cell Tracker Deep Red was simultaneously loaded in order to normalize for  
187 changes in cytosolic volume caused from cell contraction. The mean fluorescence intensity of 30 cells  
188 was averaged for Dectin-1A transfected (black) or untransfected (grey) HEK-293 cells stimulated with  
189 LMW, MMW, or HMW glucan at 1  $\mu\text{g/ml}$ . (n = 30 per glucan from 3 independent experiments per glucan).  
190 Data shown as mean fold change in volume-normalized  $[\text{Ca}^{2+}]_{\text{intracellular}}$ . (B) Heat maps of relative changes  
191 in intracellular calcium concentration of untransfected or Dectin-1A transfected individual cells upon  
192 addition of either LMW, MMW, or HMW glucan. Each row represents the normalized ratio of Fluo-4 and  
193 Cell Tracker Deep Red for a single cell over time. (C) Maximum signal amplitude of single cells treated  
194 with LMW, MMW, or HMW glucan showing Dectin-1 dependent glucan responses. Statistical comparison  
195 of maximum amplitudes for Dectin-1 expressing cells treated with each of the three glucans is shown in  
196 the far right panel. Data shown as mean  $\pm$  SD (n = 30 per glucan from 3 independent experiments per  
197 glucan). One-way ANOVA with multiple comparisons by the Dunnett test, \*\*\*  $p < 0.0001$ , \*\*\*\*  $p < 0.000001$ .  
198 (D) Cell lysates were collected at 5 min after stimulation and analyzed by Western blotting using  
199 antibodies against p-Syk and Syk. The intensity of p-Syk was normalized against total Syk. (E)  
200 Quantification of the western blot normalized p-Syk/Syk signal is shown as mean  $\pm$  SD of n = 3  
201 independent experimental replicates. (F) Untransfected (grey) and stably transfected Dectin-1A (black)  
202 HEK-293 cells were loaded with Fluo-4 and Cell Tracker Deep Red at equimolar concentrations and  
203 treated with Syk Inhibitor at 250 nM, then stimulated with MMW glucan. Average mean fluorescence  
204 intensity of 30 cells was observed for cells stimulated with MMW glucan at 1  $\mu\text{g/ml}$ . (n = 30 from 3  
205 independent experiments).

206

### 207 **$\beta$ -glucan denaturation abrogates its potential for Dectin-1A activation**

208 To determine if the glucan structure affects signaling outcomes, we denatured MMW  
209 (highly stimulatory glucan) using DMSO, a chaotrope that promotes a reduction in  
210 glucan tertiary structure, thus shifting MMW's triple helix structure to a more single  
211 helical or random coil structure [17]. The results showed that when we denatured MMW

212 glucan, we did not observe calcium signaling in cells expressing Dectin-1A (Fig. 2A, B).  
213 However, when we renatured the glucans by removing DMSO via dialysis we observe  
214 partial recovery of calcium signaling. We found that renatured glucans induce a  
215 significant increase in peak amplitude  $[Ca^{2+}]_i$  response compared to DMSO denatured  
216 MMW and renatured MMW stimulated untransfected HEK-293 cells (Fig. 2 C). In  
217 addition, we confirmed the loss of helical structure via a Congo Red assay. Congo Red  
218 specifically binds to  $\beta$ -(1,3)-glucans with a triple helix conformation as their tertiary  
219 structure. This binding is detected by bathochromic shift in absorbance maximum from  
220 488 to 516 nm [52]. Our results indicated a loss in glucan structure after denaturation in  
221 a DMSO solution that was regained upon renaturation (Fig. 2 D). Moreover, we  
222 repeated these experiments by stimulating cells with glucan denatured with NaOH or  
223 neutralized renatured glucan [17]. Similarly, our results show that cells lose the ability to  
224 activate Dectin-1A calcium signaling when stimulated with denatured MMW glucan but  
225 regain the ability to stimulate Dectin-1A activation when the glucan is renatured (Fig. 2  
226 E,F). We found that renatured glucans induce a significant increase in peak amplitude  
227  $[Ca^{2+}]_i$  response compared to NaOH denatured MMW and renatured MMW stimulated  
228 untransfected HEK-293 cells (Fig. 2 G). In addition, we confirmed that glucan structure  
229 was lost when NaOH was added and regained when neutralized (Fig. 2 H). These  
230 results suggest that glucan structure is an important factor in activating a Dectin-1A  
231 response.



232

233 **Figure 2: Glucan higher order structure is a critical determinant of its stimulatory**  
 234 **potential.**

235 (A) HEK-293 cells stably expressing Dectin-1A or untransfected were loaded with Fluo-4 and Cell Tracker  
 236 Deep Red at equimolar concentrations. Heat maps show relative changes in intracellular calcium  
 237 concentration of untransfected or Dectin-1A transfected individual cells upon either addition of DMSO  
 238 denatured MMW glucan or renatured MMW glucan. Each row represents the normalized ratio of Fluo-4  
 239 and Cell Tracker Deep Red for a single cell over time. (B) Average mean fluorescence intensity of 30 cells  
 240 stimulated with DMSO denatured/renatured MMW glucan was observed. (n = 30 from 3 independent  
 241 experiments). (C) Maximum amplitude of single cells treated with DMSO denatured or renatured MMW

242 glucan. Data shown as mean  $\pm$  SD (n = 30 from 3 independent experiments). One-way ANOVA with  
243 multiple comparisons by the Dunnett test, \*\*\*\* p<0.000001. (D) 1 mg/ml of MMW glucan was denatured  
244 using DMSO and incubated with Congo Red. Control samples contained Congo Red and DMSO.  
245 Renaturation was accomplished by dialyzing out DMSO 24 hrs prior to the experiment. Data shown as  
246 mean  $\pm$  SD (n = 9 from 3 independent experiments). (E) HEK-293 cells stably expressing Dectin-1A or  
247 untransfected were loaded with Fluo-4 and Cell Tracker Deep Red at equimolar concentrations. Heat  
248 maps show relative changes in intracellular calcium concentration of untransfected or Dectin-1A  
249 transfected cells upon either addition of NaOH denatured or renatured MMW glucan. Each row  
250 represents the normalized ratio of Fluo-4 and Cell Tracker Deep Red for a single cell over time. (F)  
251 Average mean fluorescence intensity of 30 cells stimulated with NaOH denatured/renatured MMW glucan  
252 was observed. (n = 30 from 3 independent experiments). (G) Maximum amplitude of single cells treated  
253 with NaOH denatured or renatured MMW glucan. Data shown as mean  $\pm$  SD (n = 30 from 3 independent  
254 experiments). One-way ANOVA with multiple comparisons by the Dunnett test, \*\*\*\* p<0.000001. (H) 1  
255 mg/ml of MMW glucan was denatured using NaOH and incubated with Congo Red. Control samples  
256 contained NaOH and Congo Red. Renaturation was accomplished by neutralizing NaOH. Data shown as  
257 mean  $\pm$  SD (n = 9 from 3 independent experiments). Welch's t-test, \*\* p<0.001, \*\*\* p<0.0001, \*\*\*\*  
258 p<0.000001.

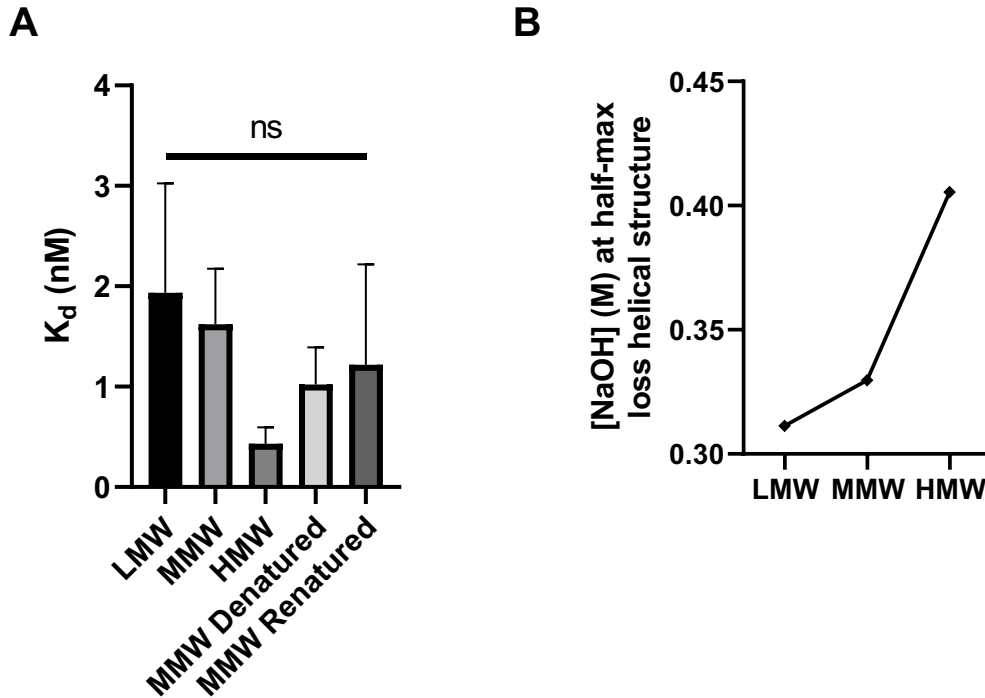
259

## 260 **$\beta$ -glucan structure variation and manipulation does not alter affinity for Dectin-1**

261 We considered the possibility that these soluble glucans might have different affinities  
262 for Dectin-1A, resulting in differential receptor activation. Thus, we conducted biolayer  
263 interferometry experiments to determine the binding affinity of these glucans to the  
264 carbohydrate recognition domain of Dectin-1A. This was accomplished using a chimeric  
265 fusion protein of the carbohydrate recognition domain of Dectin-1A and the human IgG  
266 Fc region. An anti-human IgG Fc Capture biosensor tip was used to load this fusion  
267 protein. Association and dissociation curves of the glucan and fusion protein were then

268 collected. The results shown in Fig. 3A indicate that all the glucans have approximately  
269 nanomolar dissociation constants for Dectin-1A carbohydrate recognition domain  
270 despite the previously described differences in signaling [27]. Weight average molecular  
271 weights of purified *Saccharomyces cerevisiae*  $\beta$ -(1,3)-glucan fractions vary over an  
272 approximate 40-fold range, but there is relatively little difference between these glucans'  
273 apparent affinity for the Dectin-1 carbohydrate recognition domain.  
274 Furthermore, to determine differences in the structure of these glucans, we analyzed  
275 the conformational transition of triple helix to random coil of  $\beta$ -1,3-D-glucans through  
276 denaturation experiments. Experiments were conducted by denaturing glucans with  
277 NaOH at various concentrations in the presence of Congo Red. Our results show that  
278 the amount of glucan tertiary structure scales with molecular weight as measured by the  
279 concentration of NaOH required to reduce Congo Red binding to glucan (Fig. 3B),  
280 suggesting that the size of the glucans is correlated with their higher-order structure.  
281 Together, these results indicate that downstream signaling of the receptor is determined  
282 by the structure of the glucan rather than affinity alone.





283

284 **Figure 3: Characterization of Dectin-1 binding affinity and helical structure of**  
285 **fungal cell wall glucans used in this study.**

286 (A) Biolayer interferometry experiments were conducted on LMW, MMW, HMW, MMW denatured, and  
287 MMW renatured glucans using an anti-human IgG Fc Capture biosensor tip and a Dectin-1A-Fc fusion  
288 protein. Data shown as mean  $\pm$  SD ( $n = 3$  from 3 independent experiments). Statistical comparison by  
289 one-way ANOVA. (B) LMW, MMW, and HMW  $\beta$ -glucans were denatured using 0M-1M NaOH in the  
290 presence of Congo Red. Concentration of NaOH at which absorbance (516 nm) decreased to the half-  
291 maximal value was plotted. Data shown as mean  $\pm$  SD ( $n = 9$  from 3 independent experiments).

292

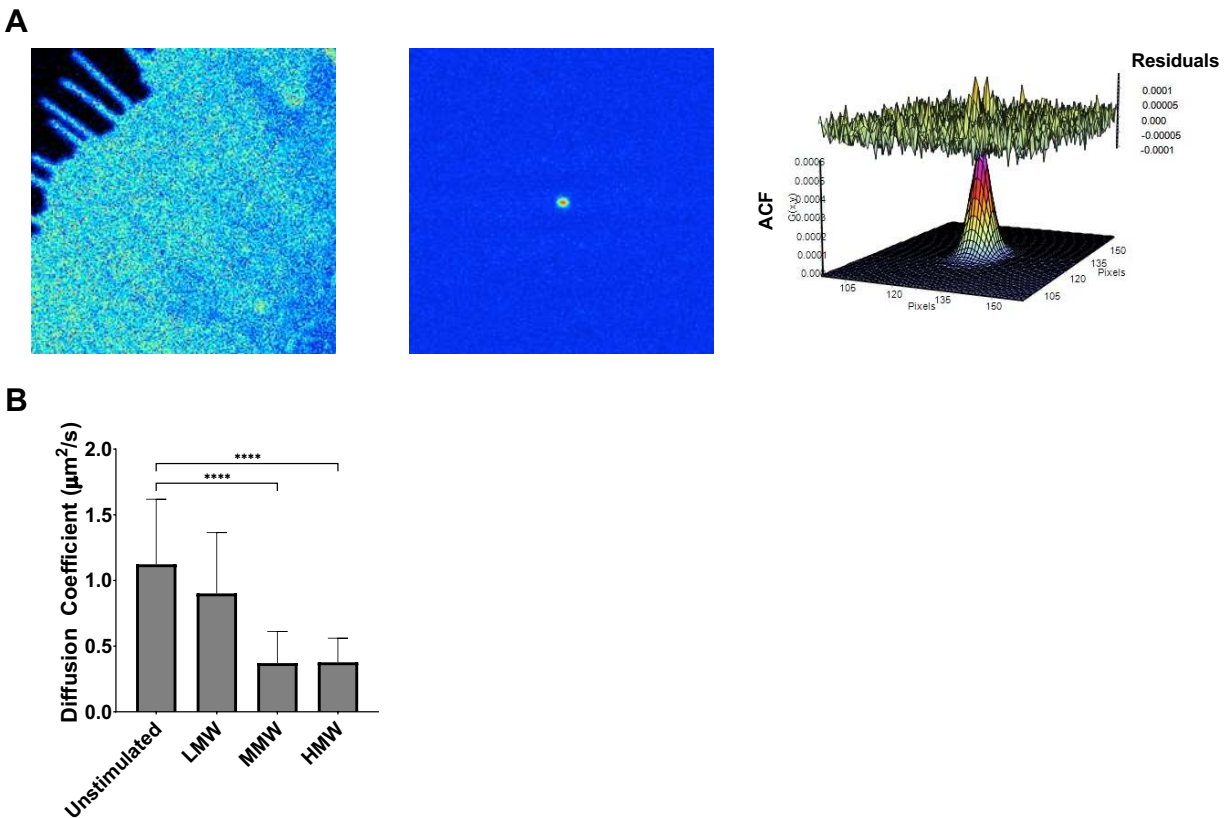
293 **Dectin-1A decreases in diffusion coefficient when stimulated with highly**  
294 **structured  $\beta$ -glucans**

295 The Stokes-Einstein equation predicts that if a diffusing object increases in  
296 hydrodynamic radius, it will slow down proportionally to that change. We measured the  
297 diffusion coefficient of Dectin-1A pre/post glucan stimulation to determine whether the

298 receptor diffusion coefficient decreased, potentially due to increasing hydrodynamic  
299 radius as an initially monomeric receptor formed larger clusters/oligomers. We obtained  
300 average diffusion coefficients and spatial number density of our receptor using Raster  
301 Image Correlation Spectroscopy (RICS). RICS allowed us to survey multiple areas of  
302 the cell for molecular parameters such as diffusion coefficient and receptor density.  
303 This section pertains to receptor diffusion measurement by RICS, while receptor density  
304 is treated in a separate section below. Furthermore, because fluorescence was probed  
305 within a large cell area, RICS analyses suffered much less from photobleaching and  
306 location specific artifacts than analogous single-point measurements. Previous research  
307 has described RICS in more detail [53,54]. Briefly, we generated a volume of excitation  
308 using focused laser illumination and calibrated a confocal observation volume using  
309 standard fluorophores of known diffusion coefficient. We observed fluorescent  
310 molecules (i.e., Dectin-1A-mEmerald) diffusing in and out of this excitation volume  
311 through fluctuation in the number of photons obtained. Experimentally observed  
312 fluorescence correlations at various spatiotemporal lags were then fit to a 2D  
313 autocorrelation function to obtain the receptor diffusion coefficient in the observed  
314 membrane (Fig. 4A).

315 Using HEK-293 cells expressing Dectin-1A-mEmerald, we conducted RICS  
316 measurements before and after stimulation with soluble  $\beta$ -glucans. We determined that  
317 cells stimulated with MMW or HMW exhibited a significant decrease in mobility  
318 compared to LMW and unstimulated cells (Fig. 4B). This finding is consistent with an  
319 increase in receptor aggregation upon stimulation, which we examine in greater detail  
320 below. We proceeded to conduct additional membrane biophysical studies to further

321 test for changes in the molecular aggregation state of Dectin-1 during stimulation with  
322 glucan.



323

324 **Figure 4: Dectin-1A surface diffusion coefficient decreases when stimulated with**  
325 **highly structured  $\beta$ -glucans.**

326 (A) A representative example of Raster Image Correlation Spectroscopy (RICS) analysis. (Left)

327 Representative RICS image of HEK-293 cells expressing Dectin-1A-mEmerald. (Middle) Autocorrelation

328 function (ACF) calculated from the time series. Red represents a high ACF value, blue represents a low

329 ACF value. (Right) Fit of the ACF to a Gaussian diffusion model to calculate the diffusion coefficient. (B)

330 RICS analysis of fluorescently tagged Dectin-1A expressed in HEK-293 provided average diffusion

331 coefficient for cells that were unstimulated or stimulated with LMW, MMW, or HMW. Data shown as mean

332  $\pm$  SD (n = 30); One-Way ANOVA multiple comparison test, \*\*\*\* p<0.00001.

333

334 **Dectin-1A forms dimers/oligomers when stimulated with highly structured  $\beta$ -**  
335 **glucans**

336 The results shown above indicate that the  $\beta$ -glucan structure is an important factor in  
337 signaling outcomes. Previous research has shown that other transmembrane CTLs that  
338 also contain a (hem)ITAM domain can form homodimers before or upon ligand  
339 recognition [55,56]. Furthermore, crystallography studies of the carbohydrate  
340 recognition domain (CRD) have shown that Dectin-1A head groups form dimers when  
341 laminaritriose is present [57]. Additionally, size exclusion chromatography with multi-  
342 angle light scattering analysis has described Dectin-1 ligand-induced tetramer (or dimer-  
343 of-dimers) formation in solution [57,58]. In line with these ideas, we sought to examine  
344 how ligand structure impacts signaling by determining the dimerization/oligomerization  
345 of full length Dectin-1A in living cell membranes.

346 To assess changing molecular proximity of Dectin-1 proteins, we employed  
347 Fluorescence Lifetime Imaging Microscopy for Forster Resonance Energy Transfer  
348 (FLIM-FRET). FRET based imaging capitalizes on close proximity of two proteins to  
349 visualize protein-protein interactions, including receptor dimerization and receptor-ligand  
350 complex formation [59]. FLIM characterizes the duration of a fluorophore's excited state  
351 before returning to the ground state. The occurrence of FRET causes rapid quenching  
352 of donor fluorescence, so FRET can be determined by measuring the shortening of  
353 donor fluorescence lifetime when in proximity to acceptor. FLIM-FRET offers the  
354 opportunity of studying *in vivo* receptor interactions in a direct, spatially resolved  
355 manner. We examined Dectin-1A engagement using FLIM-FRET on HEK-293 cells co-  
356 expressing two fluorescent Dectin-1 constructs—N-terminally tagged Dectin-1A-

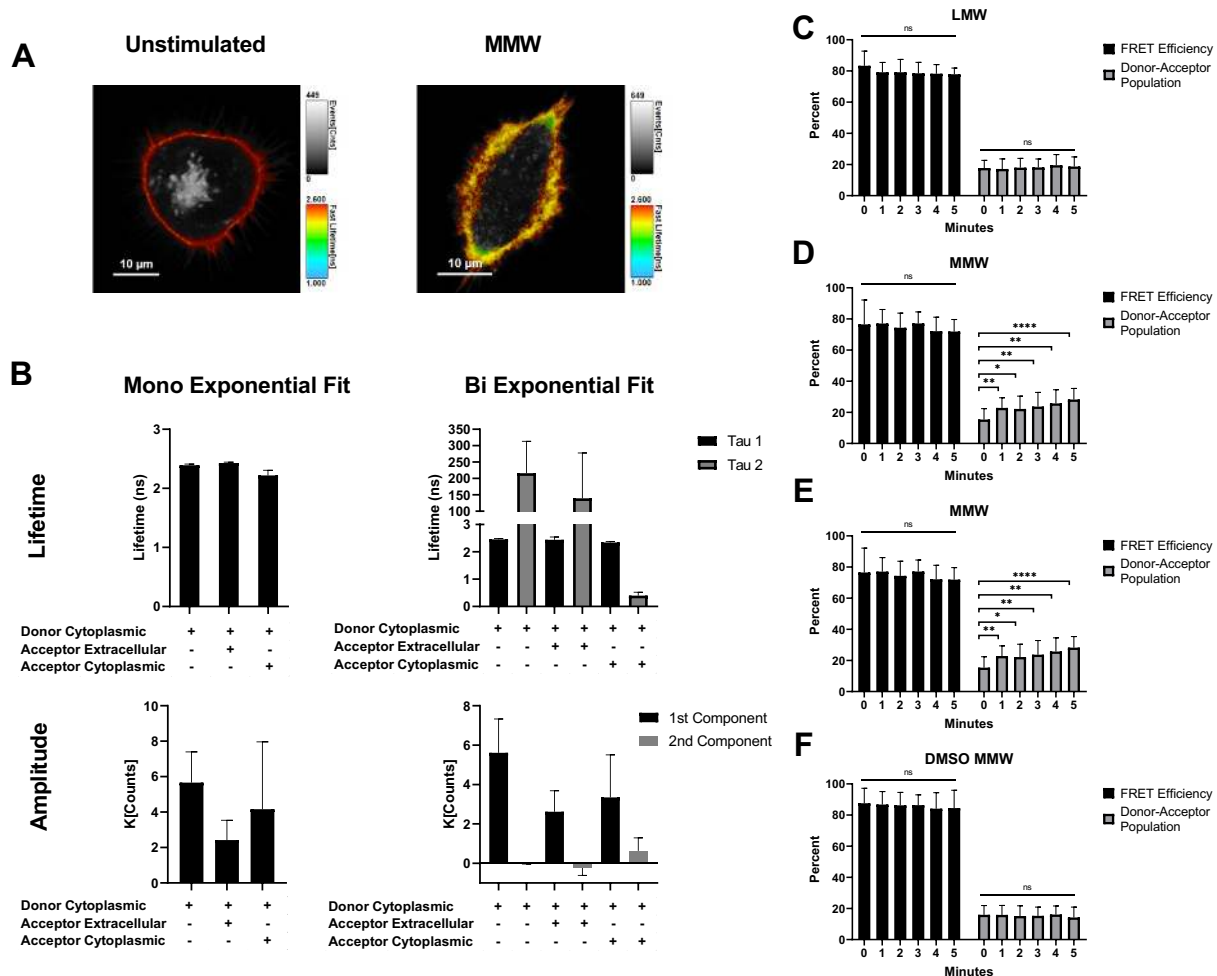
357 mEmerald (donor) and Dectin-1A-mCherry (acceptor)—both having their fluorophores  
358 on the cytoplasmic face of the plasma membrane, and then stimulated the cells with  
359 soluble  $\beta$ -glucan. Analysis was conducted on the plasma membrane itself by masking  
360 out internal cellular compartments (Fig. 5A). FRET efficiency is a parameter that  
361 exhibits an inverse 6th power dependence upon donor-acceptor distance. Donor-  
362 acceptor percentage is simply the percentage of all donors that are involved in FRET  
363 interactions at a given time. These parameters were determined experimentally by  
364 performing bi-exponential curve fits to the observed frequency distribution of donor  
365 fluorophore lifetimes, wherein one exponential component represents the population of  
366 non-FRET monomeric donors and the other exponential component represents the  
367 performance of the donors that are involved in FRET interactions.

368 First, we characterized the average lifetimes of unstimulated cells expressing several  
369 configurations of fluorescent protein tagged Dectin-1A: 1) receptor with donor tag only,  
370 2) co-expression of separate donor and acceptor tagged receptors with tags placed on  
371 opposite sides of the plasma membrane (a negative control containing both fluorescent  
372 proteins but in a configuration that does not permit FRET), and 3) co-expression of  
373 separate donor and acceptor-tagged receptors with both tags in the cytoplasmic tail of  
374 the receptors (configuration to be used for experimental determination of receptor  
375 aggregation by FRET) (Fig. 5 B). The observed decay curves were analyzed by  
376 performing a mono-exponential and bi-exponential fit. For donor only and our negative  
377 control we observed a negative amplitude for the second component in the bi-  
378 exponential fit, indicating a mono-exponential fit was superior for these conditions. This  
379 was as anticipated since these conditions should have only a single, non-FRET donor

380 signal. Additionally, the lifetimes of the second component in these controls  
381 unrealistically exceed >150 ns, further justifying a mono-exponential fit. Our results  
382 show that when acceptor is not present, we see the expected lifetime of 2.4 ns using a  
383 mono-exponential fit (Fig. 5B). Negative controls with donor and acceptor on opposite  
384 sides of the membrane yield similar lifetime values. Data from co-expression of cytosolic  
385 donor and acceptor-tagged receptor was fit bi-exponentially and the lifetime of both  
386 components is shown (Fig. 5B). We observed a decrease in the lifetime of the donor to  
387 0.41 ns (FRET-involved second fit component of a bi-exponential fit) indicating that  
388 some basal level of intermolecular Dectin-1 close proximity interactions were being  
389 observed in unstimulated cells. Of course, the first fit component lifetime (non-FRET  
390 involved donors) remained at ~2.4 ns, as expected from controls above. The existence  
391 of this basal FRET signal is interesting, and the potential sources and interpretation of  
392 this observation are further considered below. However, we first focused on assessing  
393 ligation-dependent changes in Dectin-1A's molecular aggregation state as influenced by  
394 various glucans and measured by FRET. For the remainder of the FLIM-FRET  
395 experiments, we fixed the lifetime of the first component to 2.4 ns, and we showed the  
396 second components' lifetime and amplitude values as percentages, FRET Efficiency  
397 and Donor-Acceptor Population respectively.

398 When we stimulate cells expressing Dectin-1A with donor and acceptor on the  
399 cytoplasmic face of the membrane using MMW (Fig. 5D) or HMW (Fig. 5E) glucan, we  
400 see a significant increase in the fraction of receptors undergoing FRET (Donor-Acceptor  
401 population) from 15% before stimulation to a maximum of 30% after 5 minutes of  
402 stimulation, with this trend starting at about one minute post-stimulation. However, there

403 is not a significant change in FRET efficiency before and after stimulation. On the other  
404 hand, when we stimulate with LMW (Fig. 5C) or denatured MMW (Fig. 5F), we see no  
405 significant change in FRET efficiency or donor-acceptor population. We interpret the  
406 high and constant FRET efficiency for the population of receptors engaged in FRET  
407 interactions to mean that Dectin-1A in its aggregated state is in a close configuration  
408 (e.g., dimer or tetramer) that does not permit a wide range of separations between  
409 donor and acceptor tags, leading to a constant FRET efficiency for the donor population  
410 that does attain this FRET-capable configuration. However, the size of the population of  
411 receptors engaged in these close molecular aggregates does change as a result of  
412 stimulation with glucan. These results suggest that the highly structured soluble glucans  
413 allow for an increase in Dectin-1A dimerization or oligomerization to occur, which  
414 directly correlates with the amount of receptor activation and signaling observed.



415

416 **Figure 5: Highly structured  $\beta$ -glucans induce dimerization/oligomerization of**  
 417 **Dectin-1A.**

418 (A) Representative average lifetime image of HEK-293 cell transfected with Dectin-1A-mEmerald or co-  
 419 transfected with Dectin-1A-mEmerald and Dectin-1A-mCherry. The analysis was conducted on the  
 420 plasma membrane by masking out internal cellular compartments on the images so only the masked  
 421 plasma membrane signal used for analysis is shown in color. In these images, pixel hue indicates raw  
 422 fluorescence lifetime over all populations observed and pixel intensity indicates total photon counts  
 423 observed over all populations. (B) Lifetime and amplitudes of HEK-293 cells expressing donor only on the  
 424 cytoplasmic face, donor expressed on the cytoplasmic side and acceptor on the extracellular side or  
 425 donor and acceptor placed on the cytoplasmic side of the membrane. Fluorescence decay curves were  
 426 mono- and bi-exponentially fit and individual fit components are shown. Data shown as mean  $\pm$  SD (n =

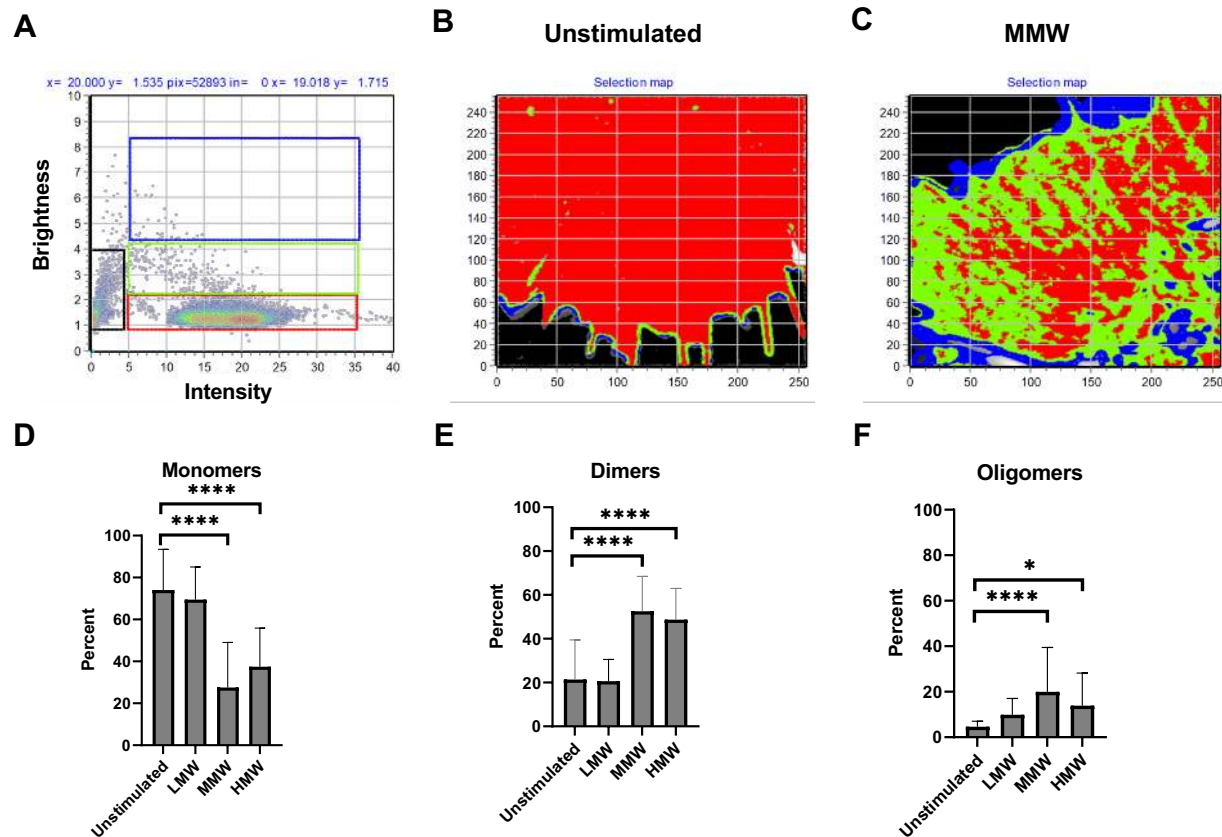


427 15 cells). (C-F) FRET efficiency and Donor-Acceptor Population of cells stimulated with LMW (C), (D)  
428 MMW, (E) HMW, or (F) DMSO denatured MMW glucan. Data shown as mean  $\pm$  SD (n = 15); One-way  
429 ANOVA with multiple comparisons by the Dunnett test, \* p<0.05, \*\*p<0.01, \*\*\*p<0.001.

430

431 In addition, to better characterize the aggregation states accessible to Dectin-1A, we  
432 conducted a Number and Brightness analysis (N&B) on HEK-293 cells expressing  
433 Dectin-1A-mEmerald. Previous research has described N&B more in depth [60–62].  
434 Briefly, N&B analysis focuses on fluctuation of detected emission photons originating  
435 from fluorescent molecules that pass through a known observation volume. Statistics of  
436 fast fluctuations of the intensity at each pixel can be used to determine the number and  
437 intensity of the particles diffusing through the observation volume. For example, if the  
438 fluorescent proteins diffuse as a tetrameric protein, we expect to observe emission  
439 intensity fluctuation with four times more photons relative to a monomeric fluorescent  
440 protein diffusing through the excitation volume. Receptor aggregation was observed by  
441 stimulating these cells with soluble glucans. A brightness vs intensity 2D histogram of  
442 each pixel in a time series was developed and selection boxes were drawn to represent  
443 monomers (red box), dimers (green box) and oligomers (blue box) (greater than dimer;  
444 Fig. 6A). Dectin-1 aggregation state maps of representative untreated (Fig. 6B) and  
445 MMW-stimulated cells (Fig. 6C) were generated using this color scheme. Our results  
446 indicated that unstimulated and LMW stimulated cells contained a significantly higher  
447 amount of monomer pixels compared to MMW and HMW glucan treated cells (Fig. 6D).  
448 Inversely, we observed a significant increase in pixels with a dimer and oligomer  
449 brightness in cells stimulated with MMW and HMW compared to cells that were

450 unstimulated or LMW stimulated (Fig. 6E, F). N&B analysis revealed that dimers of  
451 Dectin-1A account for the majority of aggregated state Dectin-1.



452

453 **Figure 6: Number and Brightness analysis shows formation of small oligomeric**  
454 **states of Dectin-1A when stimulated with highly structured  $\beta$ -glucans.**

455 (A) Brightness vs intensity 2D histogram shows the selected pixels that contribute to the background

456 (black), monomers (red), dimers (green), and oligomers (blue) in the image. (B) Representative selection

457 map of HEK-293 cells expressing Dectin-1A-mEmerald shows receptor aggregation in unstimulated cells

458 or those stimulated with (C) MMW  $\beta$ -glucan. Dectin-1 aggregation states are defined by colored boxes

459 selected in the Brightness vs intensity histogram. (D,E,F) Percentage of (D) monomers, (E) dimers, and

460 (F) oligomers in Dectin-1A-mEmerald receptors and receptor ligand complexes obtained from N&B

461 analysis before or after stimulation. Data shown as mean  $\pm$  SD (n = 30); One-way ANOVA with multiple

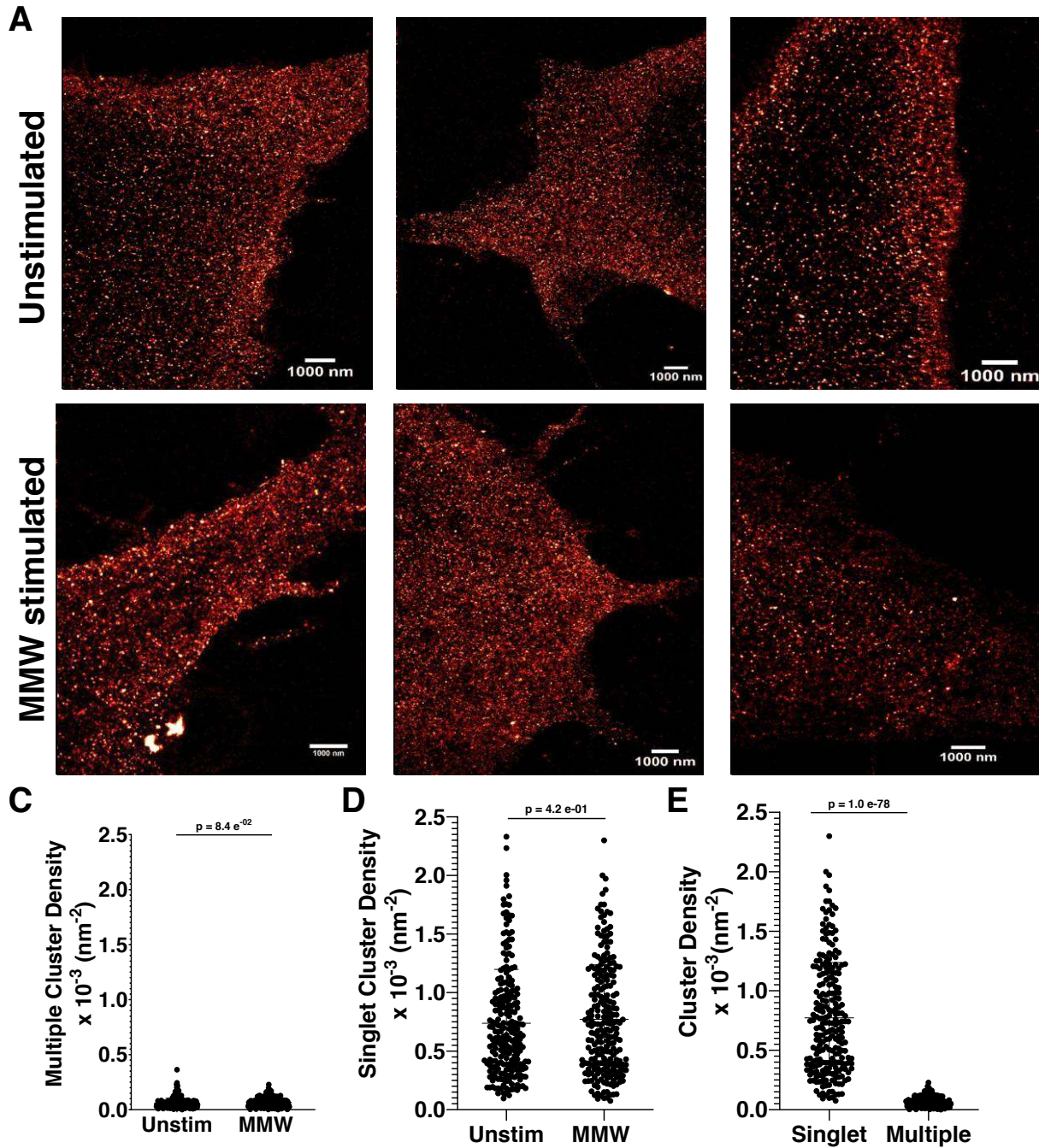
462 comparisons by the Dunnett test, \* p<0.05, \*\*\*\* p<0.00001.

463

464  **$\beta$ -glucan induced Dectin-1A aggregates are below 15 nm in size**

465 While FRET-based observations and N&B analysis clearly show the presence of ligand-  
466 induced, molecular-scale aggregation (e.g., dimerization) of Dectin-1A, these methods  
467 are not as well suited to discern the existence of larger scale aggregation of the  
468 receptor (e.g., clusters of tens to hundreds of receptors). We used direct Stochastic  
469 Optical Reconstruction Microscopy (dSTORM) coupled with Hierarchical Single-Emitter  
470 hypothesis Test (H-SET) analysis [13] to resolve aggregation of Dectin-1A before and  
471 after stimulation with MMW glucan. This localization super resolution microscopy  
472 technique accurately resolves objects from the diffraction limit (~300 nm, the resolution  
473 limit of conventional fluorescence microscopy methods) or above, down to ~15 nm (a  
474 typical resolution limit of dSTORM using our configuration). H-SET analysis detected  
475 sites of Dectin-1 labeling as “singlet” objects or “multiple” clustered objects. Multiple  
476 clustered objects are those with three or more resolvable individual Dectin-1 molecules.  
477 Singlet objects are those that appear to contain only a single, resolvable Dectin-1  
478 labeling event, though it is possible that multiple Dectin-1 molecules in very close  
479 proximity (<15 nm separation) would be unresolvable and appear as a singlet object.  
480 We detected no significant change in the density of singlet objects or multiple object  
481 clusters before vs after MMW glucan stimulation (Fig. 7A,B; Supplemental Fig. 2).  
482 Consistent with a Dectin-1 distribution of predominantly monomers or low order  
483 oligomers (likely unresolvable by dSTORM), singlet exposures greatly outnumber  
484 multiple exposures on the cell wall surface (Fig. 7C). Localization number per multiple  
485 cluster object did not change with stimulation (Supplemental Fig. 2), suggesting no

486 change in the number of receptors in this minority population of Dectin-1. In the context  
487 of the previous findings showing molecular aggregation at very small scales, potentially  
488 below the resolution limit of dSTORM, we concluded that dSTORM results indicated  
489 that the Dectin-1A aggregates formed upon glucan stimulation are quite small and  
490 remain below the resolution limit of dSTORM (<15 nm length scale). Because this  
491 places an upper bound on the size of ligand-induced Dectin-1 clusters and we can  
492 estimate that the CRD of Dectin-1 occupies an area approximately 25 nm<sup>2</sup> (PDB: 2BPD;  
493 [57,63] ), we conclude that Dectin-1 aggregation after MMW glucan stimulation most  
494 likely involves collections of not more than ~7 receptors.



495

496

497 **Figure 7: Dectin-1A does not form large scale aggregates when stimulated with**

498 **highly structured  $\beta$ -glucan.**

499 (A) Representative immunofluorescence staining images of HEK-293 cells expressing Dectin-1A and  
500 either unstimulated or stimulated with MMW  $\beta$ -glucan. Cells were stained with a conjugated anti-Dectin-1-  
501 Alexa 647 antibody. (B) Multiple cluster density of dSTORM analysis of HEK-293 cells expressing Dectin-  
502 1A unstimulated or stimulated for 50 sec with MMW glucan. (C) Singlet cluster density of dSTORM  
503 analysis of HEK-293 cells expressing Dectin-1A unstimulated or stimulated for 50 sec with MMW glucan.  
504 (D) Cluster density of singlet and multiple exposure of Dectin-1A expressing HEK-293 cells treated for 50  
505 sec with MMW glucan. Data shown as mean  $\pm$  SD (n = 34) with significance assessed by Student's T  
506 Test.

507

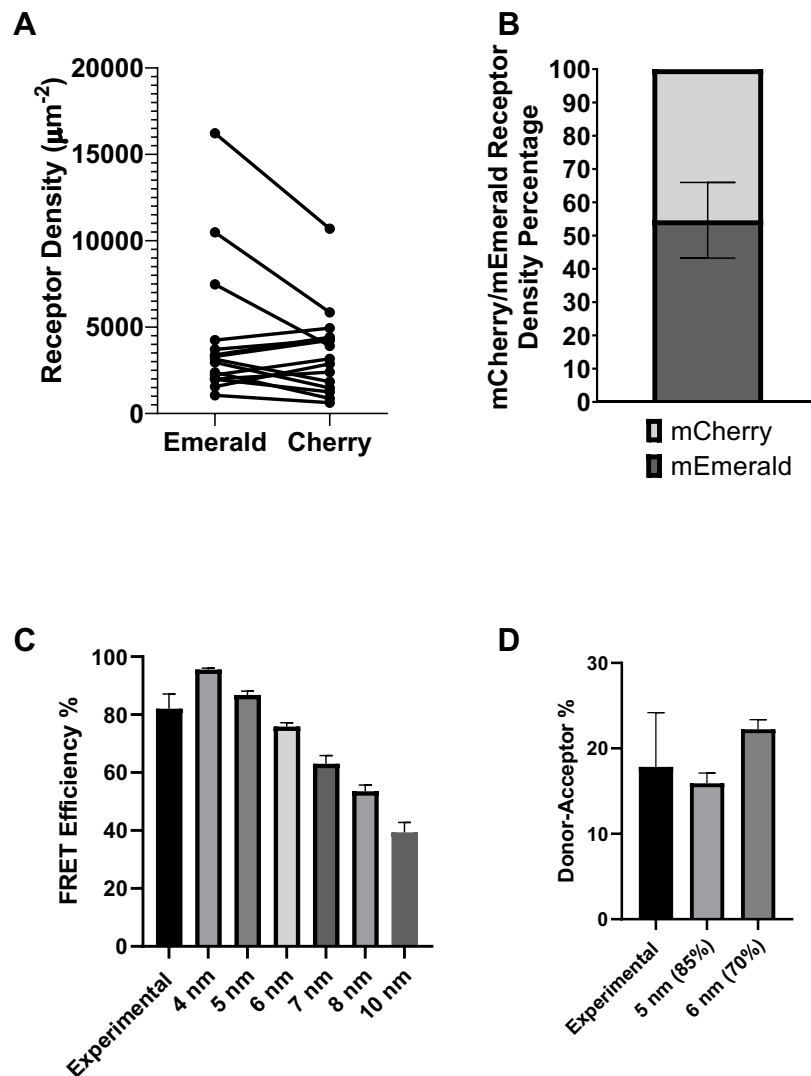
### 508 **Dectin-1A is predominantly monomeric in resting cell membranes**

509 FRET-based measurements and N&B analysis reported that the large majority of  
510 Dectin-1 is distributed as monomers in unstimulated cells. However, a minority  
511 population of apparent close-proximity receptor states was observed in resting cells by  
512 both techniques. This may represent density-dependent, close-proximity interactions  
513 between Dectin-1 molecules driven by random collisional interactions, without  
514 necessarily requiring receptor oligomer formation. Alternatively, it is possible that a  
515 small fraction of Dectin-1 does form low order oligomers, even in the absence of glucan.  
516 It is difficult to conclusively distinguish between these alternative hypotheses using only  
517 the experimental results shown above. Therefore, we created a computational model of  
518 fully monomeric Dectin-1 undergoing Brownian 2D diffusion. If such a model could  
519 predict collisional FRET interactions at a level consistent with our FRET observations in  
520 resting cells, we would conclude that random collisional interactions are sufficient to  
521 explain basal FRET observed for Dectin-1 in this study. To accurately parameterize this  
522 model, we determined the receptor density of both donor and acceptor for HEK-293  
523 cells coexpressing Dectin-1A mEmerald/mCherry by RICS analysis (Fig. 8A). Our

524 results indicated on average Dectin-1 cotransfected cells contain 54.6% mEmerald and  
525 45.4% mCherry (Fig. 8B). Therefore, our model was populated by equal proportions of  
526 donor and acceptor tagged Dectin-1 molecules. Their diffusion coefficients were  
527 parameterized using data from Fig. 4. The model calculated FRET rates for all donor-  
528 acceptor pairs within a specified maximum radial distance. The maximum radius for  
529 experimental FRET observation is limited by signal-to-noise ratio and other factors. To  
530 avoid simulating FRET measurements at experimentally unrealistic radii, we varied the  
531 model's maximum donor-acceptor radial distance for FRET calculations in a range of 4-  
532 10 nm. We compared simulated and experimental FRET efficiencies and used  
533 maximum radii for simulations that yielded FRET efficiency in best agreement with  
534 observed FRET efficiency on resting cells, indicating comparable "sensitivity" of FRET  
535 detection in both. Our results show our experimental FRET efficiency values match  
536 model predictions closely at maximum radii between 5 and 6 nm (Fig. 8C). Simulations  
537 at these chosen parameters were then compared to experimental results with respect to  
538 the donor-acceptor population percent that they predicted.

539 We used the predictions of this computational model to test the hypothesis that random  
540 collisional FRET interactions of donors and acceptors is sufficient to explain the basal  
541 FLIM-FRET signal observed experimentally in resting cells. If this model, which  
542 incorporates only collisional interactions between donors and acceptors, predicts a  
543 percent of donors undergoing FRET interactions with acceptors that match the  
544 experimentally observed value, we would consider that collisional interactions alone are  
545 sufficient to explain the observed basal FRET signal. However, if the model predicts a  
546 value significantly below that experimentally observed, we would propose that a minor

547 fraction of Dectin-1 molecules may participate in oligomeric aggregates on cell  
548 membranes, even in the absence of glucan. Using simulations with maximum radial  
549 values of 5 and 6 nm, our results indicate that the experimentally observed amount of  
550 Dectin-1 receptors dimerizing (Donor-Acceptor population) prior to stimulation match  
551 closely to our simulated results (Fig. 8D). This indicated that the FRET signal we  
552 observe prior to stimulation was attributable to random “collisional” interactions of  
553 Dectin-1A at the level of expression present in our experimental system.



554



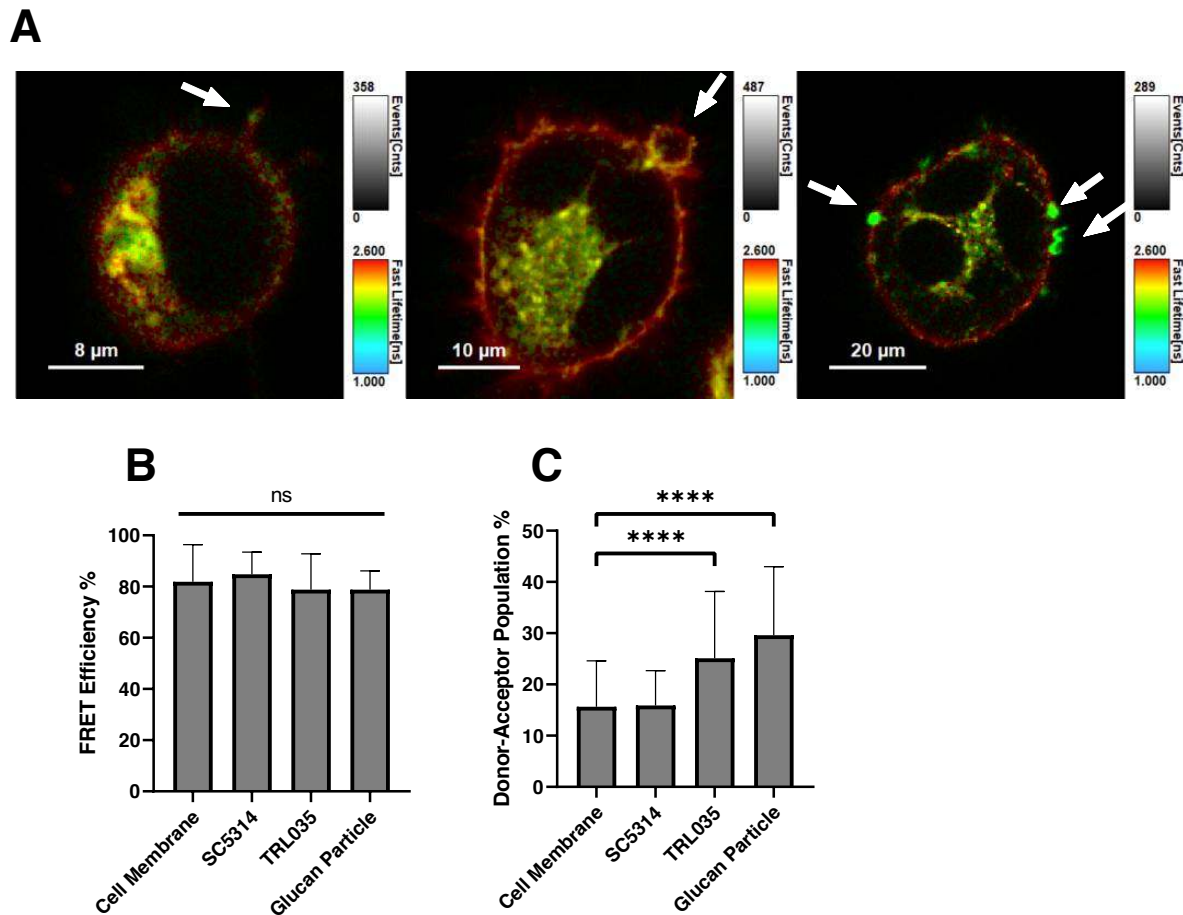
555 **Figure 8. Computational FRET modeling of monomeric Dectin-1A can account for**  
556 **basal FRET observed in Dectin-1A expressing cells.**

557 (A) Receptor density of HEK-293 cells co-expressing Dectin-1A-mEmerald and -mCherry. Lines connect  
558 paired readings from single cells. (B) Ratio of mEmerald/mCherry expression in unstimulated HEK-293  
559 cells. (C) FRET Efficiency of Dectin-1A donor/acceptor-containing computational models at different  
560 maximum intermolecular radial distances and experimental observations of FRET efficiency in resting  
561 cells for comparison. To facilitate comparison, model FRET Efficiencies are averaged over only the  
562 donors participating in non-zero FRET efficiency interactions with acceptors, and experimental FRET  
563 efficiency is derived from aggregation of all unstimulated (“0 minute”) cell data depicted in Fig. 5C-F. (D)  
564 Percentage of donors undergoing FRET (Donor-Acceptor Population) for experimentally observed  
565 populations in unstimulated cells and computational FRET modeling data at 5 and 6 nm maximum FRET  
566 radii. Experimental FRET donor-acceptor percentages were derived from aggregation of all unstimulated  
567 (“0 minute”) data in Fig. 5C-F. Data shown as mean  $\pm$  SD (n = 15 independent simulations or  
568 experimental observations on cells, respectively); One-way ANOVA multiple comparisons Dunnett test.  
569

570 **Dectin-1A dimer/oligomer and contact site formation is more efficient with cells**  
571 **incubated with *C. albicans* containing high glucan exposure.**

572 Throughout the article, we have focused on experiments using soluble glucans. In order  
573 to show Dectin-1 aggregation occurs during fungal pathogen recognition, we used a  
574 high (TRL035) and low (SC5314)  $\beta$ -glucan exposing *C. albicans* yeast and examined  
575 Dectin-1 aggregation occurring at the contact sites. TRL035 has been previously shown  
576 to have high glucan exposure compared to SC5314 [64]. In addition, our representative  
577 images show TRL035 forming a phagocytic cup more efficiently than SC5314 (Fig. 9A).  
578 Our results show that HEK-293 cells co-transfected with Dectin-1A-mEmerald and  
579 Dectin-1A-mCherry exhibit an increase in the proportion of aggregated-state receptors

580 from approximately 15% in non-contact site membrane to about 25% in contact sites of  
581 high glucan exposing yeast TRL035 and *C. albicans* derived glucan particles.  
582 Interestingly, we did not measure a significant increase in receptor aggregation between  
583 non-contact membranes and contact sites with low glucan exposing SC5314 (Fig. 9  
584 B,C), which may indicate that the amount of aggregated Dectin-1 at SC5314 contacts  
585 was quite small and below the detection limit. Furthermore, we observed no significant  
586 difference in FRET efficiency between any conditions tested (Fig. 9B), similarly to our  
587 observations with soluble glucan. The significance and interpretation of these findings is  
588 further discussed below. These results suggest that the larger cell wall glucan exposure  
589 results in an increase of Dectin-1 in molecular aggregates with associated signaling,  
590 resulting in a more efficient recognition of yeast by the Dectin-1A receptor.



591

592 **Figure 9: Dectin-1A forms more oligomers at fungal contact sites with high  $\beta$ -**  
593 **glucan exposure.**

594 (A) Representative lifetime images of HEK-293 cells co-transfected with Dectin-1A-mEmerald and Dectin-  
595 1A-mCherry incubated with SC5314 (left panel), TRL035 (middle panel) or particulate glucan (right  
596 panel). Transition from redder to greener pixels at contact sites is indicative of increased FRET  
597 interactions between Dectin-1 receptors. In these images, pixel hue indicates raw fluorescence lifetime  
598 over all populations observed and pixel intensity indicates total photon counts observed over all  
599 populations. (B) FRET efficiency and (C) donor-acceptor population of cell membranes with no fungal  
600 contact, SC5314 (low glucan exposure), TRL035 (high glucan exposure), or particulate glucan. Data  
601 shown as mean  $\pm$  SD (n = 15); One-way ANOVA with multiple comparisons by the Dunnett test, \*\*\*\*  
602 p<0.00001.

603

## 604 **Discussion**

605 Our results demonstrate that the structure of  $\beta$ -glucan impacts receptor signaling by  
606 determining the membrane organization and molecular aggregation state of Dectin-1A.  
607 We showed that glucans with higher order structure are better able to activate Dectin-  
608 1A signaling. Upon activation by stimulatory soluble glucan, Dectin-1A enters  
609 aggregated states that contain dimers and higher order oligomers, but these appear to  
610 remain as small nanoscale domains containing relatively small numbers of receptors.  
611 Comparison of computational modeling and experimental FLIM-FRET data confirms  
612 that Dectin-1A exists in a monomeric state in resting cells. Further, monomeric  
613 receptors oligomerize and aggregate in a fashion that is dependent upon glucan higher  
614 order structure and correlated with the magnitude of membrane proximal signaling  
615 downstream of Dectin-1. Finally, we observed that a similar process of increasing  
616 Dectin-1 aggregation is seen at contact sites with yeast and fungal-derived particles,  
617 and that the amount of aggregated state Dectin-1A correlates with the degree of glucan  
618 exposure on the surface of the particle.

619 The prevalence of ensemble based studies of biological response to fungal glucans,  
620 using glucans from varying sources and with varying degrees of structural  
621 characterization, has complicated a thorough understanding of the impact of glucan  
622 physicochemical properties on their biological activity. Innate immunocytes are naturally  
623 exposed to  $\beta$ -glucan in both particulate and soluble forms.  $\beta$ -glucan is widely  
624 distributed on various fungal species as an insoluble component of the cell wall. The  
625 soluble form is produced when macrophages recognize fungal surfaces and release

626 enzymes that degrade cell wall glucans [46,47]. These soluble glucans are commonly  
627 found in circulation in the serum of patients with fungal infections [48,49]. Low molecular  
628 weight glucans typically possess a random coil structure while increasing single or triple  
629 helical structure is generally seen as molecular weight increases [65]. In general,  
630 complexity of  $\beta$ -glucan correlates with immunostimulatory potency [17,27,29,65,66].  
631 Mueller, et al indicated a correlation between glucan triple helical structure and binding  
632 affinity for receptors on human promonocytic cells, which is contrary to our finding of  
633 similar affinity across glucans tested herein [27]. Discrepancies in the impact of glucan  
634 structure on affinity may be due to different cell backgrounds, or more likely, to the fact  
635 that Mueller, et al used glucans from a wide range of sources, with complex differences  
636 in structure not merely limited to size or helical content. Our study used a carefully  
637 characterized series of fungal glucans to determine that Dectin-1A activation is  
638 specifically influenced by the degree of  $\beta$ -glucan triple helical structure, not merely  
639 through its affinity or size. Furthermore, the single-cell nature of our observations  
640 suggests that the biological response to glucans with strong helical structure (e.g.,  
641 HMW glucan) seems bi-stable in nature, with response/non-response being correlated  
642 with glucan structure but the amplitude of calcium signal being similar in single cells,  
643 once successfully triggered.  
644 Aggregate states of Dectin-1 relevant to signaling could exist in a pre-formed, ligation-  
645 independent state, be formed in a purely ligation-dependent manner, or a mixture of  
646 both models. We entertained the possibility of pre-formed aggregates because receptor  
647 oligomeric states exist in the basal state for some other C-type lectin receptors, such as  
648 DCSIGN, DNGR-1, and NKp80 [67–70]. However, Dectin-1A does not contain cysteine

649 residues in its stalk region which are important in the dimerization of some other C-type  
650 lectin receptors (i.e., DNGR-1). Comparison of FRET data and computational modeling  
651 results demonstrated that any FRET activity observed in resting cells was explainable  
652 by expected levels of transient collisional donor-acceptor interactions in our cells. N&B  
653 analysis independently confirmed that the large majority of Dectin-1 is in monomeric  
654 states prior to stimulation. Therefore, we concluded that Dectin-1 is unlikely to undergo  
655 significant dimerization/oligomerization prior to ligation by glucan.

656 We proceeded to test the hypothesis Dectin-1 undergoes ligation-dependent  
657 aggregation. Specifically, we investigated whether glucan structure impacts signaling by  
658 modulating the frequency of Dectin-1A dimer/oligomer formation. Dectin-1  
659 dimerization/oligomerization would create sites where Syk could be better recruited via  
660 interactions of its SH2 domains with the (hem)ITAM phosphorylated YXXL sequence in  
661 closely juxtaposed Dectin-1A cytosolic tails. In fact, this model is commonly cited in  
662 review literature in the field, but direct evidence in intact, live cells has been lacking  
663 [71,72]. The plausibility of the Dectin-1 (hem)ITAM aggregation model is suggested by  
664 the fact that another C-type lectin receptor, CLEC-2, forms a minimal signaling unit  
665 composed of a phosphorylated dimer, enabling recruitment of a single molecule of Syk  
666 [44]. Our FLIM-FRET and N&B results reveal that Dectin-1A enters a state of greater  
667 molecular aggregation when stimulated with  $\beta$ -glucans, and that the degree of glucan  
668 helical structure correlates with its ability to induce Dectin-1 aggregation. FRET and  
669 N&B are very sensitive methods to identify receptor aggregation on the scale of small  
670 oligomers, but these methods are limited in their ability to distinguish such small  
671 aggregates from the formation of larger receptor nanodomains. dSTORM failed to

672 detect ligand inducible Dectin-1 nanodomains on a length scale of  $\geq 15$  nm, suggesting  
673 that Dectin-1 aggregation events are limited to small collections of  $\leq 7$  receptors. Our  
674 core observation of ligation-inducible Dectin-1 aggregation is directly in line with  
675 previous crystallographic studies that show monomeric Dectin-1A CRD in the absence  
676 of glucan but able to form dimeric complexes in the presence of  $\beta$ -glucan [57]. In  
677 addition, solution biophysical studies have shown a ligand-induced cooperative  
678 formation of Dectin-1 CRD tetramers (or dimers of dimers) [57,58]. However, these  
679 studies were performed with truncated receptor ectodomain proteins outside the context  
680 of living cell membranes, so our findings better establish and define the relevance of  
681 ligation-dependent Dectin-1 aggregation in a more physiologically realistic context.  
682 Nanoscale glucan exposures on *Candida* cell wall surfaces may be important  
683 determinants of the degree of Dectin-1 aggregation at host-pathogen contact sites  
684 [13,64]. Dectin-1 is recruited to the “phagocytic synapse” between innate immunocytes  
685 and fungal particles. Here, Dectin-1A encounters fungal glucan and initiates signaling  
686 [73]. We have previously described that *C. albicans* TRL035 exhibits larger glucan  
687 nanoexposures than *C. albicans* SC5314 [64]. Consistent with the presence of larger  
688 glucan exposures, we observed greater Dectin-1 aggregation at FRET contact sites with  
689 TLR035, relative to SC5314. Cell wall glucan nanoexposures are larger ( $\sim 20$ -200 nm)  
690 than the Dectin-1 aggregates generated by soluble glucans in the present work.  
691 Therefore, future studies could productively investigate the role of glucan  
692 nanoexposures in stabilizing larger aggregated collections of engaged Dectin-1, and the  
693 potential dependence of cellular activation on the scale of Dectin-1 aggregation at sites  
694 of cell wall glucan nanoexposures.

695 These and other studies improve our physical understanding of host-*Candida*  
696 interaction and highlight the exquisite sensitivity of the Dectin-1 system that drives  
697 innate immune fungal recognition. Our previous optical nanoscopy studies of *Candida*  
698 cell wall surfaces estimated multivalently-engaging glucan exposure site density and  
699 area (per exposure site) as follows: SC5314— $1 \mu\text{m}^{-2}$  density,  $6.61 \times 10^{-4} \mu\text{m}^2$  area;  
700 TRL035— $4 \mu\text{m}^{-2}$  density,  $9.62 \times 10^{-4} \mu\text{m}^2$  area [64]. The total area of contact sites  
701 between *C. albicans* and human immature dendritic cells is  $\sim 10 \mu\text{m}^2$  [74]. Finally, we  
702 estimate (see above) that one Dectin-1 CRD occupies a footprint of  $\sim 25 \text{nm}^2$ . From  
703 these figures, we calculate that a typical phagocytic synapse would contain a maximum  
704 of 264 multivalently engaged Dectin-1 proteins for *C. albicans* SC5314, and maximum  
705 385 multivalently engaged Dectin-1 for TRL035 (at total ligand engagement). Based on  
706 our reported Dectin-1 density (Fig. 4), the contact sites we measured would contain  
707  $\sim 46000$  total Dectin-1 proteins. So, the Dectin-1 system is able to drive signaling  
708 responses when, at most, only a few hundred receptors, corresponding to less than 1%  
709 of the total contact site resident Dectin-1 proteins, are aggregated in the contact. These  
710 results and estimates suggest that fungal recognition requires the Dectin-1 system to  
711 engage in a search for rare sites of multivalent interaction with glucan. Signal initiation  
712 must be sensitive to activation of relatively small numbers of Dectin-1 proteins. In the  
713 future, it will be important to achieve a better understanding of Dectin-1's collaboration  
714 with other anti-fungal receptors (e.g., DC-SIGN and CD206). Such receptors may be  
715 important for building and stabilizing a fungal contact that can effectively promote  
716 Dectin-1's ability to search for and find its rare sites of glucan exposure.



717 Overall, these findings indicate that  $\beta$ -glucan structure is required for Dectin-1A to  
718 undergo Syk-dependent signaling. Here we provide evidence in support of a model in  
719 which highly structured glucans induce stable dimerization and/or oligomerization of the  
720 receptor. This allows their (hem)ITAM domains to become close enough for a sufficient  
721 period of time to allow for the activation of Syk, leading to further signaling cascades.  
722 Greater understanding of receptor activation is required to better understand the role of  
723 Dectin-1A and its agonists as a potential way forward for adjuvant and immunotherapy  
724 development. Furthermore, given the worldwide burden of candidiasis, further  
725 experimentation is required to better understand the role of Dectin-1A in recognition of  
726 these pathogens.

727

## 728 **Materials and Methods**

### 729 **Cell Culture**

730 The HEK-293 (ATCC, #CRL-1573) cell line was maintained in Dulbecco's Minimum  
731 Essential Medium supplemented with 10% Fetal Bovine Serum (FBS), 1%  
732 penicillin/streptomycin, 2mM L-glutamine, 11mM sodium pyruvate, and 1% HEPES.  
733 Cells were grown in an incubator at 37°C at 5% CO<sub>2</sub> and saturating humidity. Cells were  
734 maintained at 37°C, 5% CO<sub>2</sub>, and 75% relative humidity during imaging.

### 735 **Plasmids and Transfection of Dectin-1 Constructs**

736 Emerald-Dectin1A-N-10(Addgene plasmid, #56291), Emerald-Dectin1A-C-10 (Addgene  
737 plasmid # 54057), mCherry-Dectin1A-C-10 (Addgene plasmid # 55025), and mCherry-  
738 Dectin1A-N-10 (Addgene plasmid # 55026) was a gift from Michael Davidson. pUNO1-  
739 hDectin-1A (Invivogen) was stably transfected into HEK-293 cells for use in our calcium

740 studies. Stable transfection of mEmerald-Dectin-1A was used for Syk immunoblotting  
741 experiments. To generate stable lines, HEK-293 cells expressing either mEmerald-  
742 Dectin-1A or pUNO-hDectin-1A were selected using Geneticin (G418 Sulfate) (Thermo-  
743 Fischer, #10131035) at 400 µg/ml or Blastidicin (Santa Cruz Biotechnology, #SC-  
744 495389) at 20 µg/ml, respectively, for 2 weeks.

745 All other experiments involving exogenous protein expression used transient  
746 transfection. Transient transfection with plasmids was performed using standard  
747 manufacturer protocols with Fugene 6 (Promega, #E2691).

#### 748 **Fungal Growth/Preparation**

749 *C. albicans* SC5314 (ATCC, MYA-2876) or TRL035 yeast cells were grown from  
750 glycerol stock, stored at -80°C. Samples were grown in YPD, for 16 h at 37°C in an  
751 orbital shaker at 250 rpm to mid log phase. Following a 3-minute centrifugation at 6000  
752 rpm, the supernatant was removed, and the cells were resuspended in 4%  
753 paraformaldehyde and sterile phosphate-buffered saline (PBS) for 15 minutes. The cells  
754 were centrifuged and washed with sterile PBS three times. The cell concentration was  
755 then determined using a disposable hemocytometer (C-Chip; Bulldog Bio catalog no.  
756 DHC-N01).  $3.5 \times 10^6$  cells were resuspended in 1 ml of PBS. 100 µl of the solution was  
757 added to HEK-293 cells in 35 mm dishes 15 minutes prior to imaging.

#### 758 **Glucan Particles**

759 Glucan microparticles were prepared from lyophilized *C. albicans* SC5314 yeast derived  
760 from stationary phase culture in YPD. Dry yeast were extracted thrice in boiling 0.75N  
761 NaOH (15 min), then residue was extracted thrice in boiling 2N H<sub>3</sub>PO<sub>4</sub> (15 min), then  
762 residue was extracted thrice in boiling acidic ethanol (1% v/v H<sub>3</sub>PO<sub>4</sub> in ethanol; 15 min),

763 and residue slurry was adjusted to neutral pH and washed thrice with ultrapure water.  
764 Pyrogen free reagent and glassware was used throughout preparation, and particles  
765 were stored at 4°C in sterile, pyrogen free water.

#### 766 **Soluble Glucan Chromatographic Analysis**

767 Low (LMW, 11 kDa), medium (MMW, 145 kDa), and high (HMW, 450 kDa) molecular  
768 weight  $\beta$ -(1,3;1-6)-glucan extracted from *S. cerevisiae* cell wall was obtained from  
769 ImmunoResearch Inc. (Eagan, MN). The molecular weight was assessed by gel  
770 permeation chromatography (GPC) and multi-angle light scattering (MALS). Samples  
771 (100  $\mu$ g) were injected and eluted with a mobile phase of 0.15 M sodium chloride  
772 containing 0.02% sodium azide at a flow rate of 0.5 mL/min using two Waters  
773 Ultrahydrogel 500 columns and one Waters Ultrahydrogel 250 column connected  
774 serially. The samples were run with the column temperature at 18°C. The Mw was  
775 calculated using Wyatt Astra software using data resulting from measurements of the  
776 angular variation of scattered light using the MALS detector coupled with the  
777 concentration measured by the refractive index signal.

#### 778 **Soluble Glucan Linkage Analysis**

779 Desalted and lyophilized samples of the fractions were dissolved in dimethylsulfoxide  
780 (DMSO) and treated with NaOH and methyl iodide to methylate all free hydroxyl groups  
781 [75]. The methylated material was purified by extraction with dichloromethane and  
782 washing with water. The purified material was then hydrolyzed with trifluoroacetic acid,  
783 the reducing ends of the resulting sugars were reduced with NaBD<sub>4</sub>, and then the  
784 resulting free hydroxyl groups were acetylated with acetic anhydride. The mixture of  
785 partially methylated alditol acetates was analyzed by gas chromatography. Each

786 derivative corresponding to a particular linkage has been identified by a characteristic  
787 retention time and mass spectrum using a mass detector. The relative amount of each  
788 derivative was measured by gas chromatography with flame ionization detection. The  
789 areas obtained for each observed peak were used to calculate the relative amounts of  
790 each type of linkage found in the sample (Table 1). The 3,6-linked residues represent  
791 branch points.

792 **Table 1.**

	LMW	MMW	HMW
Terminal Glucose	6.4	5.1	5.4
3-Glucose	87.5	87.6	84.6
3,6-Glucose	3.2	3.8	4.0
6-Glucose	1.3	2.2	3.2
4-Glucose	0.1	0.2	0.1
Other	1.5	1.1	2.7

793

#### 794 **<sup>1</sup>H NMR Spectroscopy**

795 The samples were dissolved in DMSO-d<sub>6</sub>/D<sub>2</sub>O (6:1 by volume) at 100°C for 1 h.

796 <sup>1</sup>H NMR Spectra were recorded at the University of Minnesota Department of Chemistry  
797 NMR lab on a Varian UNITYplus-300 spectrometer at 80°C. The spectra were collected  
798 at 300 MHz with 32 scans, a relaxation delay of 1.5 seconds, a pulse of 45°, an  
799 acquisition time of 2.0 seconds, and a spectral width of 5999 Hz. Table 2 provides <sup>1</sup>H  
800 NMR chemical shifts in all three glucans used in this study as well as literature values

801 [50]. These data, taken together with other characterization methods used, do confirm  
 802 that the structure of the polysaccharides used in this study conforms to expected results  
 803 from fungal cell wall glucans (Table 2, Supplemental Fig. 3).

804 **Table 2.**

	<b>H-1 (1,3- glucan)</b>	<b>H-2, 4, and 5 (1,3-)</b>	<b>H-3 and 6b (1,3-)</b>	<b>H-6a (1,3-)</b>
LMW	4.52, d, J = 7.8 Hz, 1H	3.20-3.33 m, 3H	~3.5, m, (hidden by H <sub>2</sub> O)	3.72, d, J = 11 Hz, 1H
MMW	4.52, d, J = 8.1 Hz, 1H	3.21-3.33 m, 3H	~3.5, m, (hidden by H <sub>2</sub> O)	3.72, d, J = 11 Hz, 1H
HMW	4.52, d, J = 7.8 Hz, 1H	3.20-3.32 m, 3H	~3.5, m, (hidden by H <sub>2</sub> O)	3.72, d, J = 11 Hz, 1H
Beta 1,3/1,6 Glucan Literature values	4.52, d, J = 8 Hz, 1H	3.25, m, 3H	3.46, m, 2H	3.7, d, J = 8 Hz, 1H

819 **Microscopy and Image Analysis (Calcium Imaging & RICS/N&B)**

820 Confocal images were obtained on an Olympus FV1000 laser scanning confocal  
 821 microscope (Olympus, Center Valley, PA) built around an IX81 inverted microscope. A  
 822 10x objective lens (0.40 NA) or a super corrected 60X oil objective lens (1.40 NA), Plan-  
 823 Apochromat objective lens was used for imaging. Samples were excited with a 20mW,

824 473 nm diode laser and a 20 mW, 635 nm diode laser. These lines were reflected to the  
825 specimen by a 405/473/559/635 multi-edge main dichroic element followed by  
826 bandpass emission filters in front of 2 independent High sensitivity GaAsP PMT  
827 detectors (HSD1/2). Specifically, the emission light passed by the main dichroic was  
828 directed to our first detector (HSD1) via reflection from a SDM560 filter cube and  
829 passage through a BA490-540 nm bandpass filter. Our second detector (HSD2)  
830 received light passed by the SDM560 filter cube and routed through a BA575-675 nm  
831 bandpass filter.

### 832 **Calcium Imaging**

833 HEK-293 cells expressing Dectin-1A were plated at 40,000 cells in a 35 mm (MatTEK  
834 dishes) 24 hours prior to imaging. These cells were loaded with Fluo-4 and Cell Mask  
835 Deep Red (CMDR) at equimolar concentrations of 1  $\mu$ M in 2 ml of media for one hour  
836 then washed before imaging. Cell Tracker Deep Red was used as a cell cytosolic  
837 volume control to account for cytosolic changes from cell contraction that occurs during  
838 stimulation. For Syk inhibition, plates were pre-treated with 250 nM of Syk Inhibitor  
839 (Calbiochem, #574711) for 30 min under normal growth environmental conditions.  
840 Images were taken at a resolution of 256 x 256 with a dwell time of 2  $\mu$ s on a 10x  
841 objective lens (0.40 NA). A 20 mW, 473 nm diode laser operated at 4% power and  
842 CMDR was excited with a 20 mW, 635 nm diode laser operated at 4% power.  
843 Fluorescence of Fluo-4 was collected by a cooled GaAsP PMT set to 700V, gain 1X and  
844 offset of 0%. CMDR signal was collected by a cooled GaAsP PMT detector set to 700V,  
845 gain 1X and offset of 0%. 30 frames prior to stimulation were used to set the basal  
846 fluorescence of the fluo-4 dye. After stimulation with 100  $\mu$ l of 10 $\mu$ g/ml of glucan, cells

847 were imaged for 100 frames. To assess changes in intracellular calcium concentration,  
848 we measured the ratio of Fluo-4/CMDR intensity in order to correct for any variations in  
849 cytoplasmic volume within the confocal section across the field. This ratio was  
850 normalized to 1.0 based on mean pre-stimulation values (30 frames) and changes in  
851 calcium influx were measured as fold change of this normalized ratio (MFI fold change).  
852 For MMW denaturation experiments, soluble  $\beta$ -glucans were weighed and resuspended  
853 in reverse osmosis purified H<sub>2</sub>O. In order to denature medium molecular weight glucan,  
854 we incubated MMW in DMSO or 1M NaOH. To renature the glucan from DMSO, we  
855 placed denatured MMW into Slide-A-Lyzer Dialysis Cassettes (Thermofisher, #66203)  
856 of a molecular weight cut-off of 2,000 Da and dialyzed against reverse osmosis purified  
857 H<sub>2</sub>O for 24 hours. To renature glucan from 1M NaOH, the solution was neutralized  
858 using 1M HCl.

### 859 **Protein isolation and immunoblotting**

860 HEK-293 cells stably expressing mEmerald-Dectin-1A were seeded at  $5 \times 10^5$  in 6-well  
861 plates 24 hours prior to the experiment. Cells were stimulated with Low, Medium and  
862 High molecular weight  $\beta$ -glucan (1 mg/ml) for 5 minutes, then lysed. Cells were  
863 extracted in 1X lysis buffer (43.9 mM HEPES, pH 7.5; 131.7mM NaCl; 1.1% Triton X-  
864 100; 8.8% glycerol; 1x protease inhibitor cocktail; 1mM PMSF; 1mM EGTA). Samples  
865 were centrifuged at 12,000 x g for 20 min at 4°C and supernatants transferred to fresh  
866 tubes. Protein concentrations were determined by Bradford assay (Bio-Rad Protein  
867 Reagent). NuPAGE LDS sample buffer (4X) with NuPAGE Sample Reducing agent  
868 (10X) was added to samples (1X final concentration). Total proteins (typically 20-50  $\mu$ g)  
869 were subjected to 4-12% sodium dodecyl sulfate-polyacrylamide gel electrophoresis

870 (SDS-PAGE). Proteins were transferred to Immobilon-FL PVDF transfer membrane  
871 (Millipore Sigma) using NuPAGE transfer buffer. Membranes were blocked with bovine  
872 serum albumin in Tris-buffered saline-Tween-20 (TBS-T; 20 mM Tris, 137 mM NaCl,  
873 0.1% Tween-20) and incubated with primary antibodies overnight at 4°C. Antibodies  
874 purchased from Cell Signaling: Rabbit mAb for p-SYK (Tyr525/526) and  $\beta$ -Actin (13E5),  
875 and mouse mAb Syk (4D10) were used according to manufacturer's recommendations  
876 (1:1000). HRP-conjugated anti-mouse and anti-rabbit secondary antibodies (Cell  
877 Signaling or GE Healthcare) were used at a 1:10,000 dilution. Blots were visualized on  
878 a Li-Cor Odyssey FC imaging system and analyzed with Image Studio.

### 879 **Biolayer interferometry**

880 Advanced Kinetics Biolayer interferometry experiments were conducted using the  
881 Personal Assay BLItz System. Anti-human IgG Fc Capture (AHC) Biosensors tips were  
882 initially loaded with Dectin-1A:FC fusion protein (Invivogen, #fc-hdec1a) at 13 ug/ml.  
883 Binding kinetics were obtained for LMW, MMW, HMW, MMW (denatured) and MMW  
884 (renatured) at 0, 10, 50, 100, and 250 nM in triplicate. A global fitting was performed on  
885 the curves obtained using the BLItz software.

### 886 **Congo Red Spectroscopic Assay**

887 A BioTek EON Multiwell Spectrophotometer was used to analyze Congo red  
888 absorbances. A solution of 8.8  $\mu$ M Congo Red, 0M-1M NaOH solution (1 M, 0.75 M, 0.5  
889 M, 0.25 M, 0.1 M, 0.075 M, 0.05 M, 0.025 M, 0.001 M, 0 M) and LMW, MMW, or HMW  
890  $\beta$ -glucans at 1 mg/ml were analyzed for the denaturation experiments. For the  
891 renaturation experiments, 1 mg/ml of  $\beta$ -glucan was denatured at 1M solution then  
892 renatured through neutralization with HCl 24 hrs prior to readings. DMSO denaturation



893 conditions involved DMSO in water at 0%, 5% and 10%. For the DMSO renaturation  
894 experiments, DMSO was removed by dialysis (see above) prior to spectrophotometer  
895 readings. Absorbance readings were taken at 400-700 nm with 1 nm steps. All  
896 experiments were conducted in technical triplication across three independent  
897 experimental replicates.

## 898 **Fluorescence Lifetime Imaging Microscopy and Förster Resonance Energy** 899 **Transfer Measurement**

900 HEK-293 cells were plated at 25,000 cells in a 35 mm (MatTEK dishes) 48h prior to  
901 imaging. Cells were transfected with mEmerald-Dectin1A-N-10 and mCherry-Dectin1A-  
902 N-10 24 hrs prior to imaging. FLIM-FRET images were obtained using a Leica DMI8  
903 inverted microscope. A Leica Harmonic Compound PL apochromatic CS2 63X water  
904 objective with a correction collar (1.2 NA) was used for imaging. A tunable & pulsed  
905 White Light Laser (470 - 670 nm) was operated at 80 MHz at 3% laser power using a  
906 488 nm notch filter to excite our sample. A scan speed of 200 lines/sec and a 256 x 256  
907 pixel resolution (full field of view) was used for data acquisition. Two hybrid detectors  
908 collected at photons at (512-540 nm) and (650-700 nm) respectively on the counting  
909 mode setting. Temperature was kept at 37 °C using a Tokai Hit Stage Top Incubator for  
910 Live Cell Imaging. Lifetime images were collected using a Pico Harp 300 Fluorescence  
911 Lifetime Microscopy Time-Correlated Single Photon Counting (TCSPC) system. For our  
912 glucan stimulated cells, prior to stimulation 23 frames were collected. 230 frames were  
913 taken immediately after stimulated with  $\beta$ -glucans at a concentration of 10  $\mu$ g/ml.  
914 Analysis was conducted on minute time points (1-5 minutes) by averaging ten frames  
915 from one minute intervals. For yeast contact site imaging studies,  $3.5 \times 10^6$  fixed yeast

916 cells were resuspended in 1 ml of PBS. 100  $\mu$ l of the solution was added to HEK-293  
917 cells in 35 mm dishes 15 minutes prior to imaging. 23 frames were collected per cell.  
918 Images were collected at a maximum of 45 minutes after the addition of yeast per plate.  
919 Analysis was conducted on the plasma membrane by masking out internal cellular  
920 compartments on the images. For our fungal contact site studies, analysis was  
921 conducted on the plasma membrane that was in contact with the fungus and a separate  
922 masking for plasma membrane that was not in contact with any yeast. A bi-exponential  
923 fit was performed to the decay curve. For donor only as well as donor and acceptor on  
924 opposite sides of the plasma membrane (negative control), the decay curve indicated a  
925 negative amplitude for one of the components, thus indicating a mono-exponential  
926 decay. Therefore, decay curves from these samples were analyzed using a mono-  
927 exponential fit. For cells with donor-acceptor on the cytosolic tail, data was fit to a bi-  
928 exponential decay with the first lifetime component being locked at the donor only  
929 lifetime of 2.4 ns ( $\tau_D$ ). Lifetime values of the second component ( $\tau_{DA}$ ) of the decay  
930 curve were used to calculate FRET efficiency using the equation:  $FRETEfficiency =$   
931  $\left(1 - \frac{\tau_{DA}}{\tau_D}\right) \times 100$ . To determine the fraction of receptors undergoing a FRET process  
932 (Donor-Acceptor Population), the amplitude ratio between the first component (AmpD)  
933 and the second component (AmpDA) from the bi-exponential decay curve fit was  
934 calculated according to the following formula:  $Donor - AcceptorPopulation =$   
935  $\frac{AmpDA}{(AmpD + AmpDA)} \times 100$ .

### 936 **Raster Image Correlation Analysis/Number and Brightness**

937 Protocols on RICS and N&B analysis have been previously described in more depth  
938 and analysis of diffusion coefficient and receptor density were performed using SimFCS

939 software according to these previously published procedures [54,76]. HEK-293 cells  
940 expressing Emerald-Dectin1A-C-10 were plated at 40,000 cells in a 35 mm glass  
941 bottom MatTEK dishes 24h prior to imaging using equipment described in “Microscopy  
942 and Image Analysis” section above. Measurements were performed at the membrane  
943 facing the glass coverslip. Images were collected at 256 x 256 pixel resolution on a 60×  
944 1.4 NA oil immersion objective lens with a scanning zoom of 16.4X (0.050  $\mu\text{m}$  vertical  
945 and horizontal center to center distance between resulting image pixels). Data was  
946 collected using a GaAsP PMT detector operated in photon counting mode. The 473 nm  
947 diode laser operated at 0.1% power was used in these images. The Point Spread  
948 Function (PSF) radial beam waist was estimated using 192 nM EFGP in solution and  
949 setting the diffusion coefficient to 90  $\mu\text{m}^2/\text{s}$ . Under these conditions the beam waist was  
950 determined to be 0.21  $\mu\text{m}$ . Immobile features were removed using a 4-frame moving  
951 average subtraction. Cells were stimulated with a final concentration of 1  $\mu\text{g}/\text{ml}$  of  
952 glucan. After stimulation, 200 frames were collected at a pixel dwell time of 4  $\mu\text{s}/\text{pixel}$   
953 (line scan of 1.096 ms) with a pinhole size of 100  $\mu\text{m}$ . All cell body pixels were used for  
954 analysis of N&B data from cells.

955 Images collected were also used for our Numbers and Brightness analysis; we used  
956 192 nM EGFP in solution and purified mEmerald-Dectin-1 protein to set the average  
957 brightness of our monomeric protein (Supplemental Fig. 4). Furthermore, the S-factor  
958 was calculated using the background image. We divided each brightness distribution by  
959 monomeric, dimeric, and oligomeric sections according to previous research [77]. The  
960 cursors were scaled quadratically and centered at B values of 1.3, 1.6, and 2.35 for  
961 monomers, dimers, and oligomers respectively.

962 **dSTORM**

963 HEK-293 cells, were grown on cleaned and Poly-L-Lysine (0.1 mg/ml) coated coverslips  
964 ( $\sim 5 \times 10^4$  cells/coverslip) within wells of a six-well plate at 37°C 24hrs prior to the  
965 experiment. The cells were then treated with MMW glucan at 1  $\mu$ g/ml for 50 seconds.  
966 The cells were then fixed with paraformaldehyde (PFA; 4%) for 5 minutes at 37 °C  
967 followed by three washes of PBS.

968 Data acquisition was on an Olympus IX-71 microscope equipped with an objective  
969 based TIRF illuminator using an oil-immersion objective (PlanApo N, 150 $\times$ /1.45 NA;  
970 Olympus) in an oblique illumination configuration. Sample excitation was done using a  
971 637nm laser (Thorlabs, laser diode HL63133DG), with custom-built collimation optics  
972 [13]. To minimize the drift that occurred during data acquisition, a self-registration  
973 algorithm was implemented [78,79].

974 The Dectin-1A nanodomain density by glucan exposure engagement was quantified by  
975 super resolution imaging and analyzed using H-SET as a clustering algorithm in  
976 MATLAB [13]. The data for 34 cells for each condition were run through the first pass of  
977 H-SET to collapse multiple observations of the blinking fluorophores into single  
978 estimates of the true fluorophore locations [13]. The second H-SET pass determined  
979 clustering using the DBSCAN algorithm [80] which depends on the two parameters.  
980 (minPts), that is, the minimum number of objects composing a multi-cluster, and the  
981 maximum distance between the objects within a multi-cluster (epsilon). We optimized  
982 these parameters, defining them as 3 and 27 nm, respectively, according to optimization  
983 procedures previously described [64].

984 **Collisional FRET Simulation with Monomeric Dectin-1**

985 For this simulation, first a number of particles were generated based on the number of  
986 fluorophore molecules on the membrane in a specific membrane area on the real cell.  
987 As the experiments have shown that the ratio of donors to acceptors is roughly 1:1, in  
988 our model 50% of the particles were donors while the rest were acceptors. The absolute  
989 number of donor and acceptor molecules was based on the experimentally determined  
990 Dectin-1A membrane density presented in Fig. 8.

991 The initial location of each particle in the simulation space was defined by drawing  
992 random numbers from a uniform distribution. Throughout the simulation, particle  
993 movement was modeled by using a random walk process. The distance each particle  
994 moved at each time point was determined by the diffusion coefficient that was  
995 experimentally determined and reported in Fig. 4.

996 The simulation space included monomer molecules as donors and acceptors. The size  
997 of this simulation space corresponded to an experimental area equivalent to  $0.16 \mu\text{m}^2$  of  
998 the cell membrane. The total duration of the simulation was equivalent to the total  
999 amount of time required to acquire data from 5 pixels of an experimental FLIM FRET  
1000 observation (equivalent to 24  $\mu\text{s}$  of total data acquisition time).

1001 To simulate a TCSPC FLIM experiment, each simulation run included 2000 sequential  
1002 excitation pulses, followed by a window of simulated fluorescence decay observation  
1003 with a length of 12 ns (0.1ns time resolution). At the start of each pulse, 30% of the  
1004 donors were selected to act as excited particles, which corresponded with fractional  
1005 donor excitation observed under our FLIM experimental conditions (Supplemental Fig.  
1006 5). Note that we consider that this value represents an upper bound on % donors  
1007 excited under experimental conditions due to non-linearity in response at high laser

1008 powers seen in Supplemental Figure 5, which may lead the maximum photon counts to  
1009 be an underestimate. However, FRET modeling conducted at <30% donors excited per  
1010 pulse does not violate any model assumptions nor is it mathematically expected to  
1011 yield fundamentally different results than at 30% donors excited per pulse. Moreover,  
1012 simulations run at 10% donors excited per pulse to confirm this expectation showed no  
1013 significant difference in model output (data not shown). A lifetime value was assigned to  
1014 each excited particle by generating a random number from an exponential probability  
1015 density function ( $\tau=2.4$  ns; an experimentally determined value of our donor  
1016 fluorophore). This lifetime value determined how long each excited donor remained  
1017 excited (in the absence of any FRET process).

1018 At each time point, after the new location of all particles were calculated (using a  
1019 random walk process), each excited donor neighborhood was checked for acceptors  
1020 independently. The donor's neighborhood was defined as a disk with radius of 4-10 nm.  
1021 In the case where there was an acceptor present in the region of a specific excited  
1022 donor, the energy of the donor was transferred to the acceptor, according to the rate  
1023 determined by all donor-acceptor pairs present within the above radial distance. The  
1024 FRET efficiency for a donor and a single acceptor was calculated from the following  
1025 equation:

$$E = \frac{R_0^6}{R_i^6 + R_0^6}$$

1026

1027 where  $R_0$  is the Förster distance, and  $R_i$  is the distance between donor and acceptor.  
1028 The FRET efficiency calculation is more complicated when a donor transfers its energy  
1029 to more than a single acceptor (see "FRET efficiency" below). In both cases, the donor

1030 has decayed substantially. For simplicity, the acceptors that received transferred energy  
1031 from a donor do not get excluded from receiving energy from another nearby donor. In  
1032 our models, acceptors in this condition are rare and contribute negligibly to the model  
1033 outcomes. Note that two different phenomena would result in the decay of excited  
1034 donors: FRET (as explained in this paragraph) and emission (where the excited donor  
1035 decays to ground state according to its characteristic fluorescence lifetime). The total  
1036 probability of excited state decay is the sum of probabilities from both processes.

### 1037 *FRET Efficiency Calculation (Model)*

1038 With the assumption that the concentration of excited donors is lower than the acceptor  
1039 concentration, we can consider only one donor molecule. In addition, if the orientation  
1040 factor for dipolar coupling between donor and acceptor is identical for all donor-acceptor  
1041 pairs, the FRET efficiency equation is as follows, (the pairs are considered to be  
1042 rotating freely [81]):

$$E = \frac{\sum_i^N \left(\frac{R_0}{R_i}\right)^6}{1 + \sum_i^N \left(\frac{R_0}{R_i}\right)^6}$$

1043

1044 The Förster distance ( $R_0$ ) of the pair of donor and acceptor fluorophores used for glucan  
1045 stimulation experiments also matches that used for donors and acceptors in our FLIM  
1046 FRET experiments, namely  $R_0 = 5.24$  nm [82]. The FRET efficiency in this simulation  
1047 calculates the combination of FRET resulting from acceptors surrounding one excited  
1048 donor, which are located with the specified radial distance.

### 1049 **Software**

1050 For the RICS and N&B Data presentation and analysis we used the SimFCS Program  
1051 ([www.lfd.uci.edu](http://www.lfd.uci.edu)). The calcium imaging was analyzed using ImageJ. The FLIM-FRET  
1052 results were analyzed using Symphotime64 software. The BioLayer interferometry  
1053 analysis was done using BLItz Pro software. Statistical analysis was performed with  
1054 GraphPad Prism versions 8.2 (GraphPad Software Inc.). DSTORM analysis and FLIM-  
1055 FRET modeling was performed using MATLAB using our own algorithms  
1056 (<https://github.com/NeumannLab/FRET-Simulation>).

### 1057 **Acknowledgements**

1058 The authors declare that they have no conflicts of interest relevant to this work. This  
1059 research was supported by the University of New Mexico Center for Spatiotemporal  
1060 Modeling of Cell Signaling (STMC; NIH P50GM085273, AKN) and R01AI116894 (AKN),  
1061 EUA was supported by fellowships from the STMC and an NIH T32 training grant (NIH  
1062 T32 AI007538) during the course of this work. We acknowledge the competent technical  
1063 assistance of Ms. Zinia Pervin in relation to BLI determinations of Dectin-1A/glucan  
1064 affinity. Glucans used in this study were a generous gift of Immuno Research Inc, which  
1065 played no role in experimental design, data interpretation or decision to publish. We  
1066 acknowledge use of the University of New Mexico Comprehensive Cancer Center  
1067 fluorescence microscopy shared facility, as well as the NIH P30CA118100 support for  
1068 these cores. We would like to thank the UNM Center for Advanced Research  
1069 Computing, supported in part by the National Science Foundation, for providing the high  
1070 performance computing resources used for FLIM-FRET modeling in this work.

1071

### 1072 **References**



- 1073 1. Cleveland AA, Harrison LH, Farley MM, Hollick R, Stein B, Chiller TM, et al.  
1074 Declining Incidence of Candidemia and the Shifting Epidemiology of Candida  
1075 Resistance in Two US Metropolitan Areas, 2008–2013: Results from Population-  
1076 Based Surveillance. Chowdhary A, editor. PLoS One. 2015;10: e0120452.  
1077 doi:10.1371/journal.pone.0120452
- 1078 2. Pfaller MA, Diekema DJ. Epidemiology of invasive candidiasis: a persistent public  
1079 health problem. Clin Microbiol Rev. 2007;20: 133–63. doi:10.1128/CMR.00029-06
- 1080 3. Cleveland AA, Farley MM, Harrison LH, Stein B, Hollick R, Lockhart SR, et al.  
1081 Changes in incidence and antifungal drug resistance in candidemia: results from  
1082 population-based laboratory surveillance in Atlanta and Baltimore, 2008-2011.  
1083 Clin Infect Dis. 2012;55: 1352–61. doi:10.1093/cid/cis697
- 1084 4. Kao AS, Brandt ME, Pruitt WR, Conn LA, Perkins BA, Stephens DS, et al. The  
1085 Epidemiology of Candidemia in Two United States Cities: Results of a Population-  
1086 Based Active Surveillance. Clin Infect Dis. 1999;29: 1164–1170.  
1087 doi:10.1086/313450
- 1088 5. Hajjeh RA, Sofair AN, Harrison LH, Lyon GM, Arthington-Skaggs BA, Mirza SA, et  
1089 al. Incidence of bloodstream infections due to Candida species and in vitro  
1090 susceptibilities of isolates collected from 1998 to 2000 in a population-based  
1091 active surveillance program. J Clin Microbiol. 2004;42: 1519–27.  
1092 doi:10.1128/JCM.42.4.1519-1527.2004
- 1093 6. Antibiotic Resistance Threats in the United States, 2013 | Antibiotic/Antimicrobial  
1094 Resistance | CDC [Internet]. [cited 24 Jul 2018]. Available:  
1095 <https://www.cdc.gov/drugresistance/threat-report-2013/index.html>

- 1096 7. Chaffin WL. *Candida albicans* Cell Wall Proteins. *Microbiol Mol Biol Rev.* 2008;72:  
1097 495–544. doi:10.1128/mmbr.00032-07
- 1098 8. Ruiz-Herrera J, Victoria Elorza M, Valentín E, Sentandreu R. Molecular  
1099 organization of the cell wall of *Candida albicans* and its relation to pathogenicity.  
1100 *FEMS Yeast Res.* 2006;6: 14–29. doi:10.1111/j.1567-1364.2005.00017.x
- 1101 9. Gow NAR, Hube B. Importance of the *Candida albicans* cell wall during  
1102 commensalism and infection. *Current Opinion in Microbiology.* 2012. pp. 406–  
1103 412. doi:10.1016/j.mib.2012.04.005
- 1104 10. Ballou ER, Avelar GM, Childers DS, Mackie J, Bain JM, Wagener J, et al. Lactate  
1105 signalling regulates fungal  $\beta$ -glucan masking and immune evasion. *Nat Microbiol.*  
1106 2016;2. doi:10.1038/nmicrobiol.2016.238
- 1107 11. Sherrington SL, Sorsby E, Mahtey N, Kumwenda P, Lenardon MD, Brown I, et al.  
1108 Adaptation of *Candida albicans* to environmental pH induces cell wall remodelling  
1109 and enhances innate immune recognition. *PLoS Pathog.* 2017;13.  
1110 doi:10.1371/journal.ppat.1006403
- 1111 12. Hopke A, Nicke N, Hidu EE, Degani G, Popolo L, Wheeler RT. Neutrophil Attack  
1112 Triggers Extracellular Trap-Dependent *Candida* Cell Wall Remodeling and Altered  
1113 Immune Recognition. *PLoS Pathog.* 2016;12. doi:10.1371/journal.ppat.1005644
- 1114 13. Lin J, Wester MJ, Graus MS, Lidkea KA, Neumann AK. Nanoscopic cell-wall  
1115 architecture of an immunogenic ligand in *Candida albicans* during antifungal drug  
1116 treatment. *Mol Biol Cell.* 2016;27: 1002–1014. doi:10.1091/mbc.E15-06-0355
- 1117 14. Pappas HC, Sylejmani R, Graus MS, Donabedian PL, Whitten DG, Neumann AK.  
1118 Antifungal Properties of Cationic Phenylene Ethynylenes and Their Impact on  $\beta$ -

- 1119            Glucan Exposure. *Antimicrob Agents Chemother.* 2016;60: 4519–29.  
1120            doi:10.1128/AAC.00317-16
- 1121 15.    Wheeler RT, Kombe D, Agarwala SD, Fink GR. Dynamic, morphotype-specific  
1122            *Candida albicans*  $\beta$ -glucan exposure during infection and drug treatment. *PLoS*  
1123            *Pathog.* 2008;4. doi:10.1371/journal.ppat.1000227
- 1124 16.    Wheeler RT, Fink GR. A drug-sensitive genetic network masks fungi from the  
1125            immune system. *PLoS Pathog.* 2006;2: 328–339.  
1126            doi:10.1371/journal.ppat.0020035
- 1127 17.    Sletmoen M, Stokke BT. Higher order structure of (1,3)- $\beta$ -D-glucans and its  
1128            influence on their biological activities and complexation abilities. *Biopolymers.*  
1129            2008;89: 310–321. doi:10.1002/bip.20920
- 1130 18.    Young SH, Dong WJ, Jacobs RR. Observation of a partially opened triple-helix  
1131            conformation in 1 $\rightarrow$ 3- $\beta$ - glucan by fluorescence resonance energy transfer  
1132            spectroscopy. *J Biol Chem.* 2000;275: 11874–11879.  
1133            doi:10.1074/jbc.275.16.11874
- 1134 19.    Chuah CT, Sarko A, Deslandes Y, Marchessault RH. Triple-Helical Crystalline  
1135            Structure of Curdlan and Paramylon Hydrates. *Macromolecules.* 1983;16: 1375–  
1136            1382. doi:10.1021/ma00242a020
- 1137 20.    Yoshioka Y, Uehara N, Saitô H. Conformation-dependent change in antitumor  
1138            activity of linear and branched (1----3)-beta-D-glucans on the basis of  
1139            conformational elucidation by carbon-13 nuclear magnetic resonance  
1140            spectroscopy. *Chem Pharm Bull (Tokyo).* 1992;40: 1221–6.  
1141            doi:10.1248/cpb.40.1221

- 1142 21. Okobira T, Miyoshi K, Uezu K, Sakurai K, Shinkai S. Molecular dynamics studies  
1143 of side chain effect on the  $\beta$ -1,3-D-glucan triple helix in aqueous solution.  
1144 *Biomacromolecules*. 2008;9: 783–788. doi:10.1021/bm700511d
- 1145 22. Chihara G, Hamuro J, Maeda Y, Arai Y, Fukuoka F. Fractionation and purification  
1146 of the polysaccharides with marked antitumor activity, especially lentinan, from  
1147 *Lentinus edodes* (Berk.) Sing. (an edible mushroom). *Cancer Res*. 1970;30:  
1148 2776–81. Available: <http://www.ncbi.nlm.nih.gov/pubmed/5530561>
- 1149 23. Zhou L, Zhang Q, Zhang Y, Liu J, Cao Y. The shiitake mushroom-derived  
1150 immuno-stimulant lentinan protects against murine malaria blood-stage infection  
1151 by evoking adaptive immune-responses. *Int Immunopharmacol*. 2009;9: 455–62.  
1152 doi:10.1016/j.intimp.2009.01.010
- 1153 24. Brown GD, Gordon S. Fungal  $\beta$ -glucans and mammalian immunity. *Immunity*. Cell  
1154 Press; 2003. pp. 311–315. doi:10.1016/S1074-7613(03)00233-4
- 1155 25. Novak M, Vetvicka V. )  $\beta$ -Glucans, History, and the Present: Immunomodulatory  
1156 Aspects and Mechanisms of Action. *J Immunotoxicol*. 2008;5: 47–57.  
1157 doi:10.1080/15476910802019045
- 1158 26. Kim HS, Hong JT, Kim Y, Han S-B. Stimulatory Effect of  $\beta$ -glucans on Immune  
1159 Cells. *Immune Netw*. 2011;11: 191. doi:10.4110/in.2011.11.4.191
- 1160 27. Mueller a, Raptis J, Rice PJ, Kalbfleisch JH, Stout RD, Ensley HE, et al. The  
1161 influence of glucan polymer structure and solution conformation on binding to (1--  
1162 >3)-beta-D-glucan receptors in a human monocyte-like cell line. *Glycobiology*.  
1163 2000;10: 339–346. doi:10.1093/glycob/10.4.339
- 1164 28. Zhang L, Li X, Xu X, Zeng F. Correlation between antitumor activity, molecular

- 1165 weight, and conformation of lentinan. *Carbohydr Res.* 2005;340: 1515–21.  
1166 doi:10.1016/j.carres.2005.02.032
- 1167 29. Elder MJ, Webster SJ, Chee R, Williams DL, Hill Gaston JS, Goodall JC.  $\beta$ -glucan  
1168 size controls dectin-1-mediated immune responses in human dendritic cells by  
1169 regulating IL-1 $\beta$  production. *Front Immunol.* 2017;8.  
1170 doi:10.3389/fimmu.2017.00791
- 1171 30. Di Luzio NR, Williams DL, McNamee RB, Edwards BF, Kitahama A. Comparative  
1172 tumor-inhibitory and anti-bacterial activity of soluble and particulate glucan. *Int J*  
1173 *cancer.* 1979;24: 773–9. doi:10.1002/ijc.2910240613
- 1174 31. Tzianabos AO. Polysaccharide immunomodulators as therapeutic agents:  
1175 structural aspects and biologic function. *Clin Microbiol Rev.* 2000;13: 523–33.  
1176 doi:10.1128/cmr.13.4.523-533.2000
- 1177 32. Wang Y, Zhang L, Li Y, Hou X, Zeng F. Correlation of structure to antitumor  
1178 activities of five derivatives of a  $\beta$ -glucan from *Poria cocos sclerotium*. *Carbohydr*  
1179 *Res.* 2004;339: 2567–2574. doi:10.1016/j.carres.2004.08.003
- 1180 33. Smith AJ, Graves B, Child R, Rice PJ, Ma Z, Lowman DW, et al.  
1181 Immunoregulatory Activity of the Natural Product Laminarin Varies Widely as a  
1182 Result of Its Physical Properties. *J Immunol.* 2018;200: 788–799.  
1183 doi:10.4049/jimmunol.1701258
- 1184 34. Suzuki T, Ohno N, Saito K, Yadomae T. Activation of the complement system by  
1185 (1---3)-beta-D-glucans having different degrees of branching and different  
1186 ultrastructures. *J Pharmacobiodyn.* 1992;15: 277–85. Available:  
1187 <http://www.ncbi.nlm.nih.gov/pubmed/1432567>

- 1188 35. Maeda YY, Watanabe ST, Chihara C, Rokutanda M. Denaturation and  
1189 renaturation of a beta-1,6;1,3-glucan, lentinan, associated with expression of T-  
1190 cell-mediated responses. *Cancer Res.* 1988;48: 671–5. Available:  
1191 <http://www.ncbi.nlm.nih.gov/pubmed/2446749>
- 1192 36. Yanaki T, Ito W, Tabata K, Kojima T, Norisuye T, Takano N, et al. Correlation  
1193 between the antitumor activity of a polysaccharide schizophyllan and its triple-  
1194 helical conformation in dilute aqueous solution. *Biophys Chem.* 1983;17: 337–  
1195 342. doi:10.1016/0301-4622(83)80018-0
- 1196 37. Duggan S, Leonhardt I, Hünninger K, Kurzai O. Host response to *Candida albicans*  
1197 bloodstream infection and sepsis. *Virulence.* 2015; 1–11.  
1198 doi:10.4161/21505594.2014.988096
- 1199 38. Davis SE, Hopke A, Minkin SC, Montedonico AE, Wheeler RT, Reynolds TB, et  
1200 al. Masking of  $\beta(1-3)$ -glucan in the cell wall of *Candida albicans* from detection by  
1201 innate immune cells depends on phosphatidylserine. *Infect Immun.* 2014;82:  
1202 4405–13. doi:10.1128/IAI.01612-14
- 1203 39. Gow NAR, Netea MG, Munro CA, Ferwerda G, Bates S, Mora-Montes HM, et al.  
1204 Immune recognition of *Candida albicans* beta-glucan by dectin-1. *J Infect Dis.*  
1205 2007;196: 1565–71. doi:10.1086/523110
- 1206 40. Brown GD, Taylor PR, Reid DM, Willment JA, Williams DL, Martinez-Pomares L,  
1207 et al. Dectin-1 is a major  $\beta$ -glucan receptor on macrophages. *J Exp Med.*  
1208 2002;196: 407–412. doi:10.1084/jem.20020470
- 1209 41. Rice PJ, Adams EL, Ozment-Skelton T, Gonzalez AJ, Goldman MP, Lockhart BE,  
1210 et al. Oral delivery and gastrointestinal absorption of soluble glucans stimulate

- 1211 increased resistance to infectious challenge. *J Pharmacol Exp Ther.* 2005;314:  
1212 1079–86. doi:10.1124/jpet.105.085415
- 1213 42. O'Neill SK, Getahun A, Gauld SB, Merrell KT, Tamir I, Smith MJ, et al.  
1214 Monophosphorylation of CD79a and CD79b ITAM motifs initiates a SHIP-1  
1215 phosphatase-mediated inhibitory signaling cascade required for B cell anergy.  
1216 *Immunity.* 2011;35: 746–756. doi:10.1016/j.immuni.2011.10.011
- 1217 43. Tomohiro Kurosaki B, AJohnson S, Pao L, Sada K, HiroheYamamura II, Cambier  
1218 JC. Role of the Syk Autophosphorylation Site and SH2 Domains in B Cell Antigen  
1219 Receptor Signaling. doi:10.1084/jem.182.6.1815
- 1220 44. Hughes CE, Pollitt AY, Mori J, Eble JA, Tomlinson MG, Hartwig JH, et al. CLEC-2  
1221 activates Syk through dimerization. *Blood.* 2010;115: 2947–55.  
1222 doi:10.1182/blood-2009-08-237834
- 1223 45. Bartel Y, Bauer B, Steinle A. Modulation of NK cell function by genetically coupled  
1224 C-type lectin-like receptor/ligand pairs encoded in the human natural killer gene  
1225 complex. *Front Immunol.* 2013;4: 362. doi:10.3389/fimmu.2013.00362
- 1226 46. Hino S, Kito A, Yokoshima R, Sugino R, Oshima K, Morita T, et al. Discharge of  
1227 solubilized and Dectin-1-reactive  $\beta$ -glucan from macrophage cells phagocytizing  
1228 insoluble  $\beta$ -glucan particles: Involvement of reactive oxygen species (ROS)-driven  
1229 degradation. *Biochem Biophys Res Commun.* 2012;421: 329–334.  
1230 doi:10.1016/j.bbrc.2012.04.009
- 1231 47. Hong F, Yan J, Baran JT, Allendorf DJ, Hansen RD, Ostroff GR, et al. Mechanism  
1232 by which orally administered beta-1,3-glucans enhance the tumoricidal activity of  
1233 antitumor monoclonal antibodies in murine tumor models. *J Immunol.* 2004;173:

- 1234 797–806. doi:10.4049/jimmunol.173.2.797
- 1235 48. Gonzalez JA, Digby JD, Rice PJ, Breuel KF, DePonti WK, Kalbfleisch JH, et al. At  
1236 low serum glucan concentrations there is an inverse correlation between serum  
1237 glucan and serum cytokine levels in ICU patients with infections. *Int*  
1238 *Immunopharmacol.* 2004;4: 1107–1115. doi:10.1016/J.INTIMP.2004.05.010
- 1239 49. Digby J, Kalbfleisch J, Glenn A, Larsen A, Browder W, Williams D. Serum glucan  
1240 levels are not specific for presence of fungal infections in intensive care unit  
1241 patients. *Clin Diagn Lab Immunol.* 2003;10: 882–5. doi:10.1128/cdli.10.5.882-  
1242 885.2003
- 1243 50. Kim YT, Kim EH, Cheong C, Williams DL, Kim CW, Lim ST. Structural  
1244 characterization of  $\beta$ -D-(1  $\rightarrow$  3, 1  $\rightarrow$  6)-linked glucans using NMR spectroscopy.  
1245 *Carbohydr Res.* 2000;328: 331–341. doi:10.1016/S0008-6215(00)00105-1
- 1246 51. Kogan G, Alföldi J, Masler L.  $^{13}\text{C}$ -nmr spectroscopic investigation of two yeast  
1247 cell wall  $\beta$ -D-glucans. *Biopolymers.* 1988;27: 1055–1063.  
1248 doi:10.1002/bip.360270702
- 1249 52. Nitschke J, Modick H, Busch E, von Rekowski RW, Altenbach H-J, Mölleken H. A  
1250 new colorimetric method to quantify  $\beta$ -1,3-1,6-glucans in comparison with total  $\beta$ -  
1251 1,3-glucans in edible mushrooms. *Food Chem.* 2011;127: 791–796.  
1252 doi:10.1016/J.FOODCHEM.2010.12.149
- 1253 53. Brown CM, Dalal RB, Hebert B, Digman MA, Horwitz AR, Gratton E. Raster  
1254 image correlation spectroscopy (RICS) for measuring fast protein dynamics and  
1255 concentrations with a commercial laser scanning confocal microscope. *J Microsc.*  
1256 2008;229: 78–91. doi:10.1111/j.1365-2818.2007.01871.x



- 1257 54. Digman MA, Stakic M, Gratton E. Raster image correlation spectroscopy and  
1258 number and brightness analysis. *Methods Enzymol.* 2013;518: 121–44.  
1259 doi:10.1016/B978-0-12-388422-0.00006-6
- 1260 55. Bauer B, Steinle A. HemITAM: A single tyrosine motif that packs a punch. *Sci*  
1261 *Signal.* 2017;10: 1–10. doi:10.1126/scisignal.aan3676
- 1262 56. Brown GD. Dectin-1: a signalling non-TLR pattern-recognition receptor. *Nat Rev*  
1263 *Immunol.* 2006;6: 33–43. doi:10.1038/nri1745
- 1264 57. Brown J, O’Callaghan CA, Marshall ASJ, Gilbert RJC, Siebold C, Gordon S, et al.  
1265 Structure of the fungal beta-glucan-binding immune receptor dectin-1: implications  
1266 for function. *Protein Sci.* 2007;16: 1042–52. doi:10.1110/ps.072791207
- 1267 58. Dulal HP, Adachi Y, Ohno N, Yamaguchi Y.  $\beta$ -Glucan-induced cooperative  
1268 oligomerization of Dectin-1 C-type lectin-like domain. *Glycobiology.* 2018;28: 612–  
1269 623. doi:10.1093/glycob/cwy039
- 1270 59. Singh DR, Kanvinde P, King C, Pasquale EB, Hristova K. The EphA2 receptor is  
1271 activated through induction of distinct, ligand-dependent oligomeric structures.  
1272 *Commun Biol.* 2018;1: 15. doi:10.1038/s42003-018-0017-7
- 1273 60. Digman MA, Dalal R, Horwitz AF, Gratton E. Mapping the number of molecules  
1274 and brightness in the laser scanning microscope. *Biophys J.* 2008;94: 2320–32.  
1275 doi:10.1529/biophysj.107.114645
- 1276 61. Unruh JR, Gratton E. Analysis of molecular concentration and brightness from  
1277 fluorescence fluctuation data with an electron multiplied CCD camera. *Biophys J.*  
1278 2008;95: 5385–98. doi:10.1529/biophysj.108.130310
- 1279 62. Trullo A, Corti V, Arza E, Caiolfa VR, Zamai M. Application limits and data

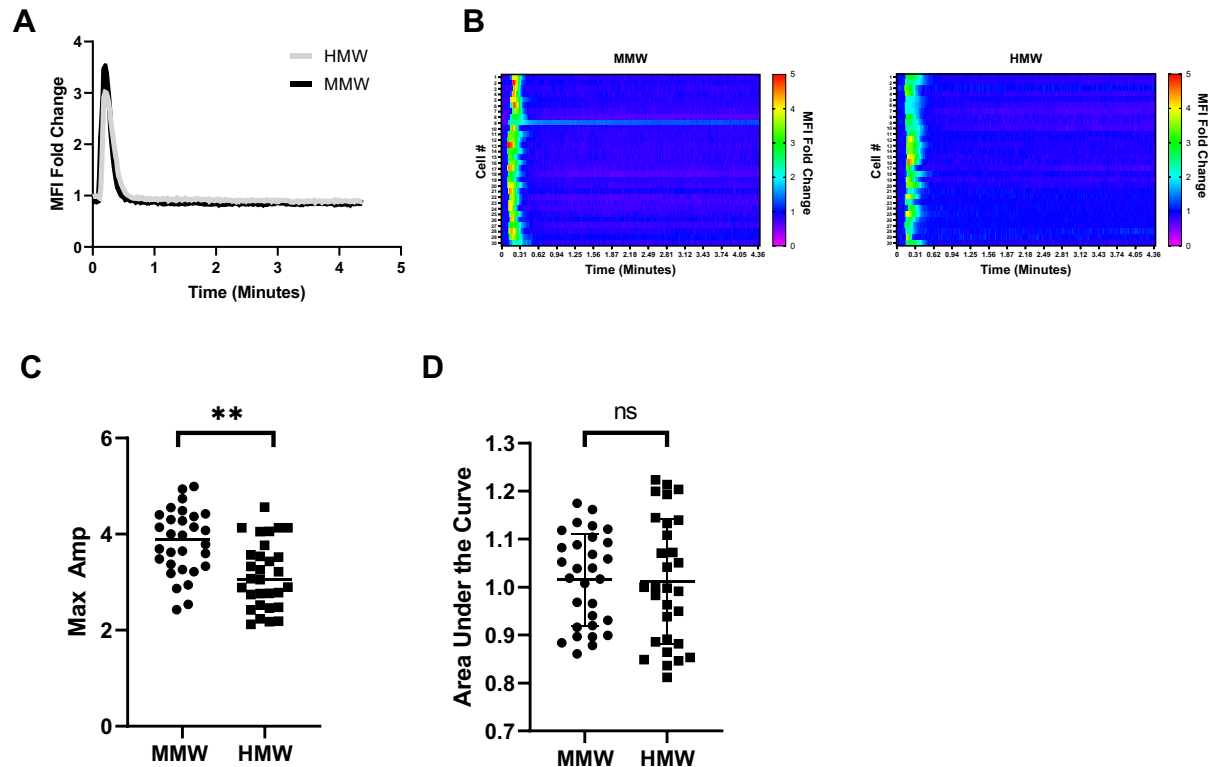
- 1280 correction in number of molecules and brightness analysis. *Microsc Res Tech.*  
1281 2013;76: 1135–1146. doi:10.1002/jemt.22277
- 1282 63. Wester MJ, Lin J, Neumann AK. A computational model for regulation of  
1283 nanoscale glucan exposure in *Candida albicans*. *PLoS One.* 2017;12.  
1284 doi:10.1371/journal.pone.0188599
- 1285 64. Graus MS, Wester MJ, Lowman DW, Williams DL, Kruppa MD, Martinez CM, et  
1286 al. Mannan Molecular Substructures Control Nanoscale Glucan Exposure in  
1287 *Candida*. *Cell Rep.* 2018;24: 2432-2442.e5. doi:10.1016/j.celrep.2018.07.088
- 1288 65. Okazaki M, Adachi Y, Ohno N, Yadomae T. Structure-Activity Relationship of  
1289 (1,3)- $\beta$ -D-Glucans in the Induction of Cytokine Production from  
1290 Macrophages, in Vitro. *Biol Pharm Bull.* 1995;18: 1320–1327.  
1291 doi:10.1248/bpb.18.1320
- 1292 66. Cleary JA, Kelly GE, Husband AJ. The effect of molecular weight and  $\beta$ -1,6-  
1293 linkages on priming of macrophage function in mice by (1,3)- $\beta$ -d -glucan.  
1294 *Immunol Cell Biol.* 1999;77: 395–403. doi:10.1046/j.1440-1711.1999.00848.x
- 1295 67. Itano MS, Graus MS, Pehlke C, Wester MJ, Liu P, Lidke KA, et al. Super-  
1296 resolution imaging of C-type lectin spatial rearrangement within the dendritic cell  
1297 plasma membrane at fungal microbe contact sites. *Front Phys.* 2014;2.  
1298 doi:10.3389/fphy.2014.00046
- 1299 68. Feinberg H, Guo Y, Mitchell DA, Drickamer K, Weis WI. Extended neck regions  
1300 stabilize tetramers of the receptors DC-SIGN and DC-SIGNR. *J Biol Chem.*  
1301 2005;280: 1327–35. doi:10.1074/jbc.M409925200
- 1302 69. Vitale M, Falco M, Castriconi R, Parolini S, Zambello R, Semenzato G, et al.

- 1303 Identification of NKp80, a novel triggering molecule expressed by human NK  
1304 cells. *Eur J Immunol.* 2001;31: 233–242. doi:10.1002/1521-  
1305 4141(200101)31:1<233::AID-IMMU233>3.0.CO;2-4
- 1306 70. Hanč P, Schulz O, Fischbach H, Martin SR, Kjær S, Reis e Sousa C. A pH- and  
1307 ionic strength-dependent conformational change in the neck region regulates  
1308 DNGR-1 function in dendritic cells. *EMBO J.* 2016;35: 2484–2497.  
1309 doi:10.15252/emj.201694695
- 1310 71. Schorey JS, Lawrence C. The Pattern Recognition Receptor Dectin-1: From  
1311 Fungi to Mycobacteria. *Curr Drug Targets.* 2008;9: 123.
- 1312 72. Marakalala MJ, Kerrigan AM, Brown GD. Dectin-1: A role in antifungal defense  
1313 and consequences of genetic polymorphisms in humans. *Mamm Genome.*  
1314 2011;22: 55–65. doi:10.1007/s00335-010-9277-3
- 1315 73. Goodridge HS, Reyes CN, Becker CA, Katsumoto TR, Ma J, Wolf AJ, et al.  
1316 Activation of the innate immune receptor Dectin-1 upon formation of a “phagocytic  
1317 synapse”. *Nature.* 2011;472: 471–5. doi:10.1038/nature10071
- 1318 74. Graus MS, Pehlke C, Wester MJ, Davidson LB, Steinberg SL, Neumann AK. A  
1319 New Tool to Quantify Receptor Recruitment to Cell Contact Sites during Host-  
1320 Pathogen Interaction. Gabhann F Mac, editor. *PLoS Comput Biol.* 2014;10:  
1321 e1003639. doi:10.1371/journal.pcbi.1003639
- 1322 75. Needs PW, Selvendran RR. Avoiding oxidative degradation during sodium  
1323 hydroxide/methyl iodide-mediated carbohydrate methylation in dimethyl sulfoxide.  
1324 *Carbohydr Res.* 1993;245: 1–10. doi:10.1016/0008-6215(93)80055-J
- 1325 76. Youker RT, Teng H. Measuring protein dynamics in live cells: protocols and

- 1326 practical considerations for fluorescence fluctuation microscopy. *J Biomed Opt.*  
1327 2014;19: 090801. doi:10.1117/1.jbo.19.9.090801
- 1328 77. Planes N, Digman MA, Vanderheyden PPML, Gratton E, Caballero-George C.  
1329 Number and brightness analysis to study spatio-temporal distribution of the  
1330 angiotensin II AT1 and the endothelin-1 ETA receptors: Influence of ligand  
1331 binding. *Biochim Biophys Acta - Gen Subj.* 2019;1863: 917–924.  
1332 doi:10.1016/J.BBAGEN.2019.03.004
- 1333 78. Smith CS, Joseph N, Rieger B, Lidke KA. Fast, single-molecule localization that  
1334 achieves theoretically minimum uncertainty. *Nat Methods.* 2010;7: 373–375.  
1335 doi:10.1038/nmeth.1449
- 1336 79. Huang F, Schwartz SL, Byars JM, Lidke KA. Simultaneous multiple-emitter fitting  
1337 for single molecule super-resolution imaging. *Biomed Opt Express.* 2011;2: 1377.  
1338 doi:10.1364/boe.2.001377
- 1339 80. Ester M, Ester M, Kriegel H-P, Sander J, Xu X. A density-based algorithm for  
1340 discovering clusters in large spatial databases with noise. *AAAI Press.* 1996; 226-  
1341 -231. doi=10.1.1.121.9220
- 1342 81. Nyitrai M, Hild G, Lukács A, Bódis E, Somogyi B. Conformational distributions and  
1343 proximity relationships in the rigor complex of actin and myosin subfragment-1. *J*  
1344 *Biol Chem.* 2000;275: 2404–2409. doi:10.1074/jbc.275.4.2404
- 1345 82. Akrap N, Seidel T, Barisas BG. Förster distances for fluorescence resonant  
1346 energy transfer between mCherry and other visible fluorescent proteins. *Anal*  
1347 *Biochem.* 2010;402: 105–106. doi:10.1016/J.AB.2010.03.026
- 1348



## 1350 Supplemental Materials



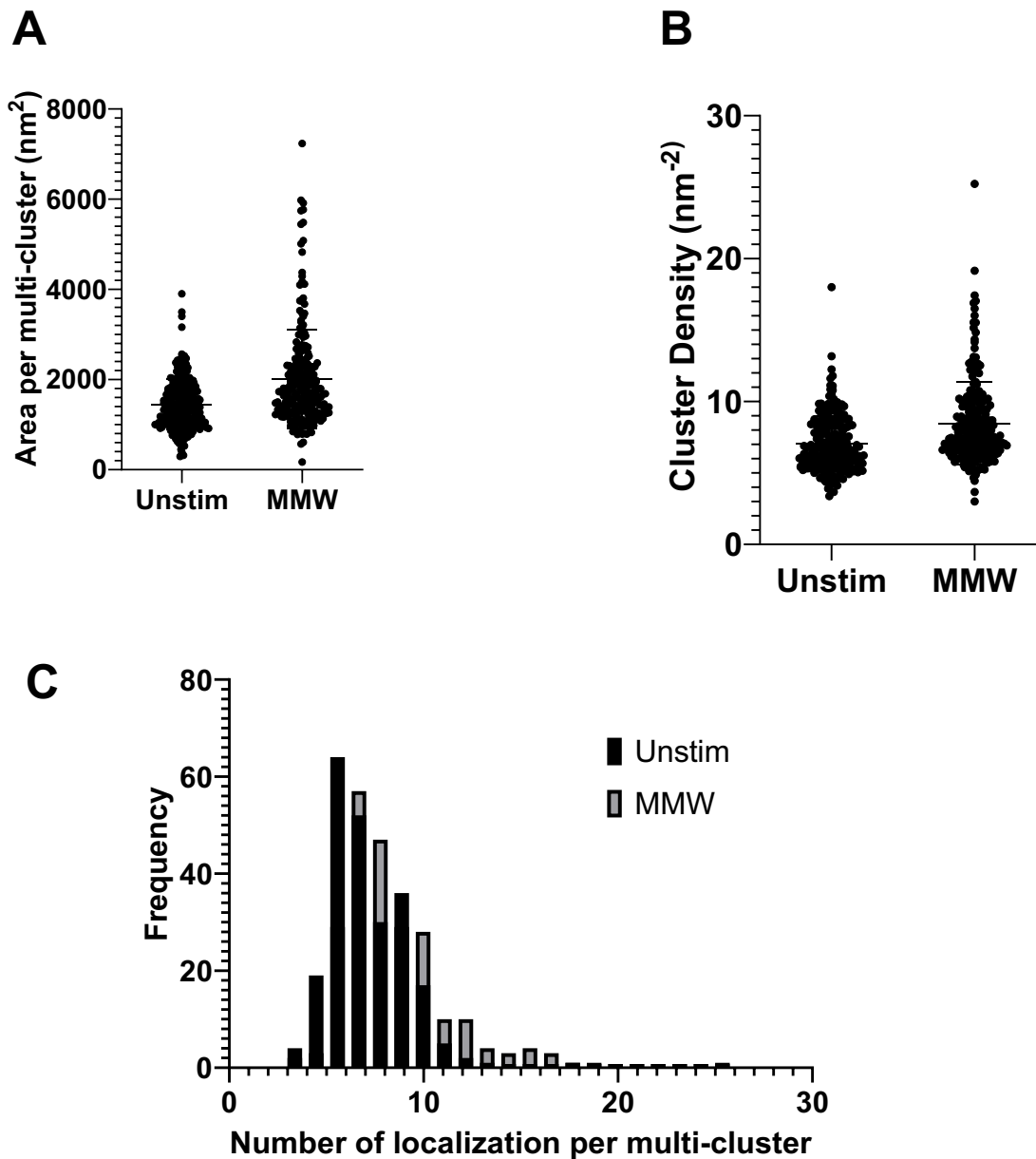
1351

## 1352 Supplemental Figure 1. Equimolar glucan stimulation of Dectin-1A exhibits 1353 similar response to MMW and HMW glucans

1354 (A) HEK-293 cells stably transfected with Dectin-1A were loaded with Fluo-4 and Cell Tracker Deep Red  
1355 at equimolar concentrations. Cell Tracker Deep Red was simultaneously loaded in order to normalize for  
1356 changes in cytosolic volume caused from cell contraction. The mean fluorescence intensity of 30 cells  
1357 was averaged for Dectin-1A transfected HEK-293 cells stimulated with MMW or HMW glucan at 6.67 nM.  
1358 (n = 30 per glucan from 3 independent experiments per glucan). Data shown as mean fold change in  
1359 volume-normalized  $[Ca^{2+}]_{intracellular}$ . (B) Heat maps show relative changes in intracellular calcium  
1360 concentration of Dectin-1A transfected individual cells upon either addition of MMW or HMW glucan.  
1361 Each row represents the normalized ratio of Fluo-4 and Cell Tracker Deep Red for a single cell over time.  
1362 (C) Maximum amplitude of single cells treated with MMW or HMW glucan, as depicted in panel B. Data  
1363 shown as mean  $\pm$  SD (n = 30 cells); Welch's t-test, \*\* p<0.001 (D) Area under the curve of individual

1364 traces of MMW or HMW glucan stimulated cells, as depicted in panel B. Data shown as mean  $\pm$  SD (n =  
1365 30 cells).  
1366

1367



1368

1369 **Supplemental Figure 2. dSTORM clustering analysis shows similar multicluster**  
1370 **characteristics in unstimulated and stimulated cells.**

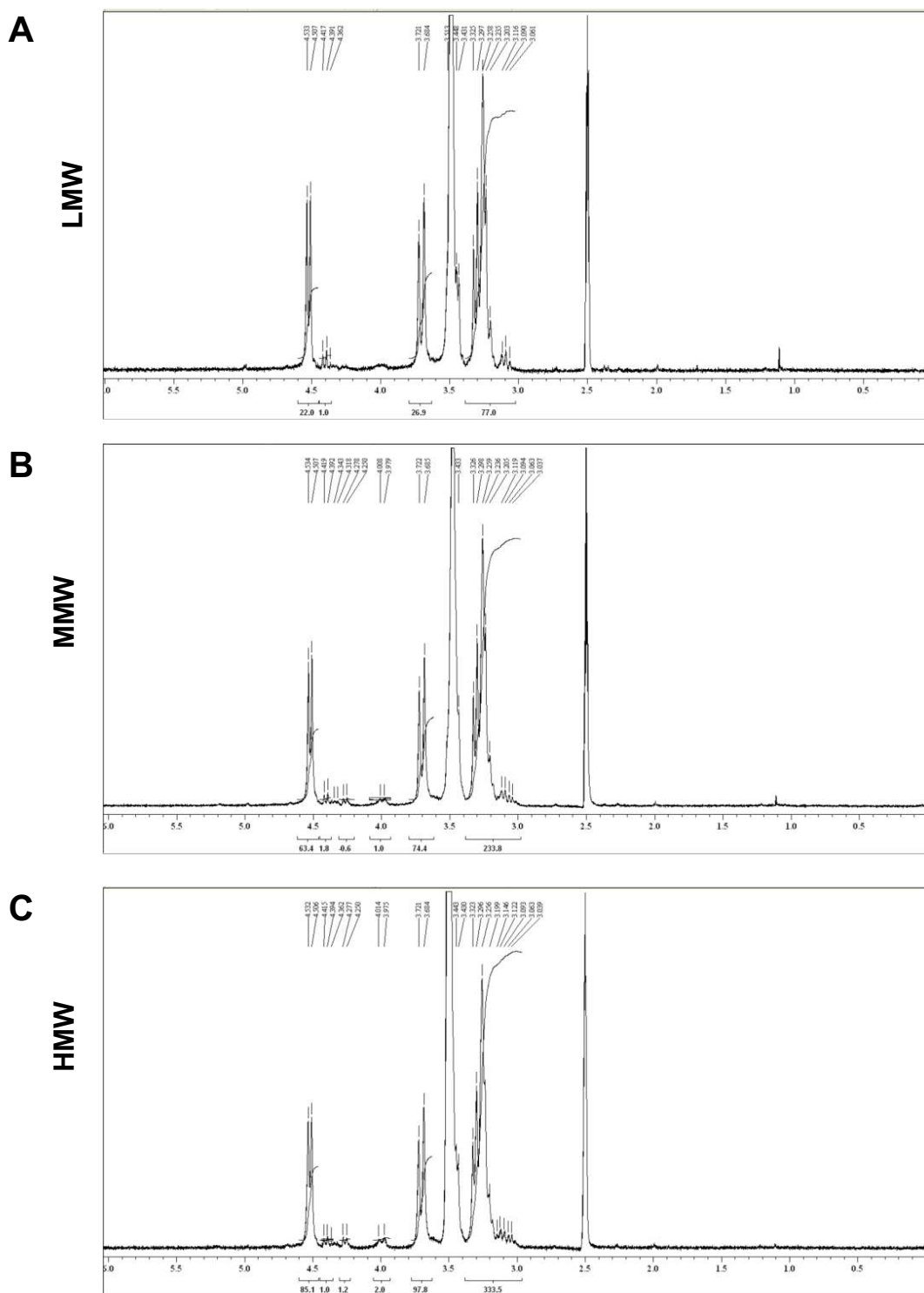
1371 (A) Areas per multi-cluster in dSTORM analysis of HEK-293 cells expressing Dectin-1A unstimulated or

1372 stimulated with MMW. (B) Cluster density of dSTORM analysis of HEK-293 cells expressing Dectin-1A



1373 unstimulated or stimulated with MMW. (C) Histogram analysis of the number of localizations of HEK-293  
1374 cells expressing Dectin-1A unstimulated or stimulated with MMW. Data shown as mean  $\pm$  SD (n = 34).  
1375

1376

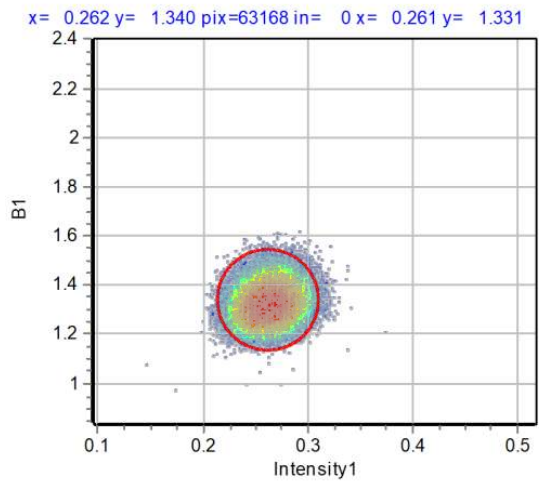


1377

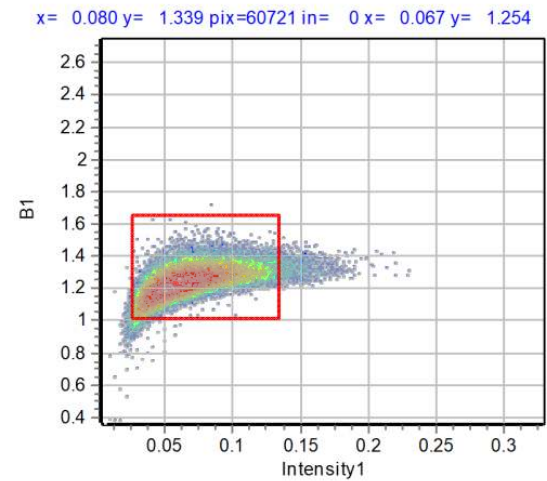
1378 **Supplemental Figure 3.  $^1\text{H}$ NMR spectra of glucans used in this study.**

1379 (A)  $^1\text{H}$  NMR spectrum of LMW, (B) MMW, and (C) HMW glucan.

**A**



**B**

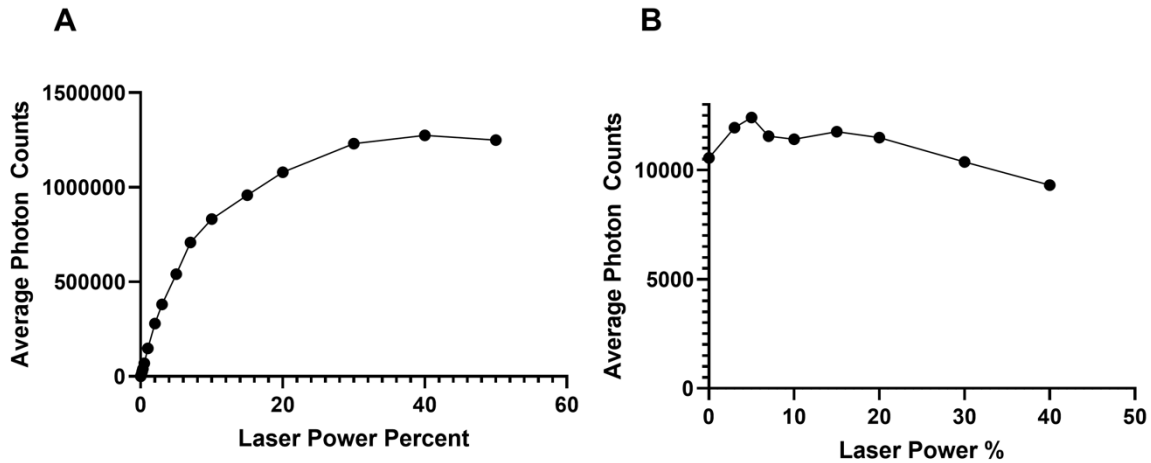


1380

1381 **Supplemental Figure 4. Numbers and Brightness analysis calibration.**

1382 (A) Brightness vs intensity 2D histogram of purified EGFP with the selected pixels that contribute to the  
1383 monomers (red circle) in the image. A brightness value of 1.34 was obtained. (B) Brightness vs intensity  
1384 2D histogram of purified mEmerald-Dectin-1A with the selected pixels that contribute to the monomers  
1385 (red box) in the image. A brightness value of 1.34 was obtained.

1386



1387

1388 **Supplemental Figure 5. Estimation of fractional donor population excited under**  
1389 **FLIM FRET experimental conditions.**

1390 (A) Average photon counts from cells expressing mEmerald-Dectin-1A were obtained at  
1391 different excitation laser powers using all other experimental conditions as described in  
1392 Methods (“Fluorescence Lifetime Imaging Microscopy” section). Maximum photon  
1393 counts were considered to approximate 100% donor excitation and the percent of  
1394 donors excited at 3% laser power (the excitation intensity used for experiments) was  
1395 obtained using the following equation:

1396 
$$\frac{\text{PhotonCounts at 3\% laser Power}}{\text{Maximum Photon Counts}} \times 100$$

1397 and was used to parameterize the FRET model. (B) To check for possible  
1398 photobleaching during acquisition of data in (A), average photon counts were separately  
1399 acquired (excitation at 0.1% laser power) after each laser power data point in (A) was  
1400 acquired, from each individual cell. Photobleaching was negligible across the  
1401 experiments conducted to obtain data in (A).

1402 **Supplemental Table 1.**

Table of Values								
	LMW		MMW		HMW			
Max Calcium Amplitude	1.3 ± 0.1295		3.4 ± 0.3378		1.9 ± 0.3837			
	LMW	MMW	HMW	MMW Denatured	MMW Renatured			
Kd (nM)	1.93 ± 1.09	1.62 ± 0.55	0.43 ± 0.17	1.02 ± 0.37	1.22 ± 1.00			
	LMW		MMW		HMW		MMW Denatured	
Min	FRET Efficiency %	Donor-Acceptor %	FRET Efficiency %	Donor-Acceptor %	FRET Efficiency %	Donor-Acceptor %	FRET Efficiency %	Donor-Acceptor %
0	83.3 ± 9.50	17.7 ± 4.97	76.5 ± 15.69	15.3 ± 7.02	86.1 ± 7.48	14.5 ± 4.66	87.5 ± 9.69	15.9 ± 5.97
1	79.1 ± 6.31	17.1 ± 6.48	77.0 ± 9.05	22.8 ± 6.54	80.1 ± 9.05	19.5 ± 5.49	86.7 ± 8.36	15.8 ± 6.06
2	79.1 ± 8.28	17.9 ± 5.98	74.3 ± 9.39	22.1 ± 8.25	78.9 ± 8.89	19.8 ± 6.20	86.2 ± 8.36	15.1 ± 6.63
3	78.5 ± 7.03	18.1 ± 5.41	77.1 ± 7.43	23.7 ± 9.13	78.9 ± 8.90	21.7 ± 6.91	86.3 ± 6.66	15.2 ± 5.68
4	78.2 ± 5.85	19.5 ± 6.89	72.1 ± 9.05	25.7 ± 8.87	79.5 ± 8.12	22.5 ± 5.40	84.1 ± 10.29	16.1 ± 5.51

5	77.9 ± 3.96	18.8 ± 6.16	71.9 ± 7.76	28.2 ± 7.12	79.5 ± 9.14	23.7 ± 8.16	84.5 ± 11.45	14.1 ± 6.70
N&B								
RICS								
	Monomers %	Dimers %	Oligomers %	Diffusion Coefficient (μm <sup>2</sup> /s)				
Unstimulated	74.0 ± 19.47	21.4 ± 18.09	4.6 ± 2.39	1.12 ± 0.50				
LMW	69.5 ± 15.59	20.6 ± 9.94	9.9 ± 7.15	0.90 ± 0.46				
MMW	27.5 ± 21.56	52.5 ± 15.93	20.0 ± 19.49	0.37 ± 0.24				
HMW	37.5 ± 18.44	48.7 ± 14.24	13.8 ± 14.35	0.37 ± 0.18				
Singlet Cluster								
	Singlet Cluster Density (nm <sup>-2</sup> )	Multiple Cluster Density (nm <sup>-2</sup> )	Density of Localizations (nm <sup>-2</sup> )	Area per cluster(nm <sup>2</sup> )				
Unstimulated	0.74 ± 0.46	0.59 ± 0.05	7.06 ± 1.95	1444 ± 559				
MMW	0.77 ± 0.46	0.66 ± 0.04	8.47 ± 2.87	2016 ± 1093				
FRET Efficiency %								
	FRET Efficiency %					Donor- Acceptor %		
Cell Membrane	81.8 ± 14.53					15.7 ± 8.97		
SC5314	84.8 ± 8.67					15.9 ± 6.78		
TRL035	78.8 ± 13.98					25.1 ± 13.06		
Glucan Particle	78.8 ± 7.33					29.6 ± 13.36		